European Commission
H2020 Programme for Research & Innovation

Advanced monitoring, simulation and control of tidal devices in unsteady, highly turbulent realistic tide environments

Grant Agreement number: 727689

Project Acronym: RealTide

Project Title: Advanced monitoring, simulation and control of tidal devices in unsteady, highly turbulent realistic tide environments

WP 3
Realistic simulation of tidal turbines

Deliverable 3.4
Inter-comparison of BEMT, Blade-Resolved CFD, and BEMT-CFD Hybrid Models of scale turbines

WP Leader: The University of Edinburgh (UEDIN)

Dissemination level: Public

Summary: Tidal turbines can make an important contribution to low carbon energy generation, particularly in remote areas with weak electricity grids. The energetic waters in which they are deployed are not only characterised by fast flowing currents, but also large-scale turbulence and large waves. This complex environment leads to dynamic loading on the blades and drive train of the turbines which must be accounted for by designers. The European RealTide project aims to deepen understanding of the environment and support turbine developers. As part of the project the utility of using Blade Element Momentum Theory (BEMT) based design tool [StarBlades], Computational Fluid Dynamics (CFD) solvers with BEMT actuator line models of the turbine blades [SOWFA] and blade resolved CFD solvers [STAR-CCM+] is being investigated. Each requires an order of magnitude more computational effort but provides greater fidelity. In this paper we present an inter-comparison of the three approaches with experimental data obtained from tests conducted on a 1:15 generic, 3-bladed, horizontal axis, model turbine and a 1:20 model of the Sabella D12 5-bladed turbine. The capability of the approaches to predict important turbine performance parameters including thrust, torque and root bending moment is discussed along with a spectral analysis of the time-series output. This analysis shows that turbulence models and models of wave inducted fluid motion are critical to obtaining high quality simulations. Based on this analysis we make recommendations on the most suitable tools to simulating tidal turbines to understand loading and key design parameters. This will allow designers to develop more robust turbines thus both increasing reliability and reducing maintenance costs, giving tidal turbines a competitive Levelized Cost Of Energy (LCOE).

Objectives:

- Compare the numerical models' outputs using experimental test results obtained in IFREMER and FloWave tank tests.
- Assess the ability of each model to predict turbines' loads and performances.
- Determine the strengths, weakness and applicability of each modelling approach

Abbreviations & Definitions

ADV	Acoustic Doppler Velocitymeter
ALM	Actuator Line Model
BEMT	Blade Element Momentum Theory
CFD	Computational Fluid Dynamics
CFL	Courant-Friedrichs-Lewy
CPU	Central Processing Unit
DES	Detached Eddy Simulation
FMEA	Failure Mode and Effects Analysis
FVM	Finite Volume Method
HAT	Horizontal Axis Turbine
IFREMER	Institut Français de Recherche pour l'Exploitation de la MER
ITTC	International Towing Tank Conference
LDV	Lase Doppler Velocitymeter
LES	Large Eddy Simulations
NACA	National Advisory Committee for Aeronautics
PISO	Pressure Implicit Splitting Operation
RANSE	Reynolds Averaged Navier-Stokes Equations
RBM	Rigid Body Motion / Root Bending Moment
ReDAPT	Reliable Data Acquisition Platform for Tidal
RFM	Reference Frame Motion
RPM	Rotations Per Minute
SFS	Sub-Filter Scale
SOWFA	Simulator fOr Wind Farm Applications
SST	Shear Stress Transport
TEC	Tidal Energy Converter
TI	Turbulence Intensity
TSR	Tip Speed Ratio
UEDIN	University of EDINburgh

Contents

List of Figures

List of Tables

The Inter-comparison of BEMT, Blade-Resolved CFD, and BEMT-CFD Models of scale turbines

C.P. Old, A. Ortega, D. Ingram
School of Engineering
The University of Edinburgh

J.Marcille, B. Battaglia
Research and Development Dept.
Sabella

J.P. Tomy
Composite Materials Section, Dept. of Expertise
Bureau Veritas Marine & Offshore

S. Loubeyre
Fluid Dynamics Dept.
Bureau Veritas Solutions Marine & Offshore

April 2020

Abstract

Tidal turbines can make an important contribution to low carbon energy generation, particularly in remote areas with weak electricity grids. The energetic waters in which they are deployed are not only characterised by fast flowing currents, but also large scale turbulence and large waves. This complex environment leads to dynamic loading on the blades and drive train of the turbines which must be accounted for by designers. The European RealTide project aims to deepen understanding of the environment and support turbine developers. As part of the project the utility of using Blade Element Momentum Theory (BEMT) based design tool [StarBlades], Computational Fluid Dynamics (CFD) solvers with BEMT actuator line models of the turbine blades [SOWFA] and blade-resolved CFD solvers [STAR-CCM+] is being investigated. Each requires an order of magnitude more computational effort, but provides greater fidelity. In this paper we present an inter-comparison of the three approaches with experimental data obtained from tests conducted on a 1:15 generic, 3-bladed, horizontal axis, model turbine and a 1:20 model of the Sabella D12 5-bladed turbine. The capability of the approaches to predict important turbine performance parameters including thrust, torque and root bending moment is discussed along with a spectral analysis of the time-series output. This analysis shows that turbulence models and models of wave inducted fluid motion are critical to obtaining high quality simulations. Based on this analysis we make recommendations on the most suitable tools to simulating tidal turbines to understand loading and key design parameters. This will allow designers to develop more robust turbines thus both increasing reliability and reducing maintenance costs, giving tidal turbines a competitive Levelized Cost Of Energy (LCOE).

Keywords: tidal turbine, numerical simulation, BEMT, blade-resolved CFD, BEMT-CFD, tank testing, inter-comparison, realistic conditions, loads, performance

Acknowledgements

Many thanks to Dr. Brian Sellar from the University of Edinburgh for their valuable inputs and suggestions that directly contributed to the redaction of this paper.

The work presented hereafter received funding from the European Union's Horizon 2020 research and innovation programme under the RealTide project linked to grant agreement No 727689.

1 Introduction

The tidal energy sector is a growing industry and is considered a regular, predictable and dense energy source with potential to make a significant contribution to our future energy needs. By 2050 tidal energy could meet 10 % of European electricity requirements [1]. But the risks associated with these relatively young technologies are not yet fully understood and often lead to a lack of confidence from potential investors. One of the

main challenges is to improve the reliability of tidal turbines to reduce the risks, attract investors and reduce construction and maintenance costs.

The flow characteristics of tidal sites typically vary across flood and ebb tides, feature significant spatial variation across temporal scales in all three directions and are heavily impacted by waves and wave-current interaction. Work for the ReDAPT project (2010-2015, see `http://www.redapt.eng.ed.ac.uk`) showed that under non-extreme wave conditions power fluctuations on a commercial-prototype 1MW tidal energy converter (TEC) were of the order of 30% of rated power per wave cycle. Experiments in combined wave-current conditions in test-tanks have also demonstrated the strong influence of waves on rotor and turbine loading [2].

In the design stage, tidal developers use the loads induced by extreme environmental conditions to size the different elements of tidal turbines. These sub-systems include bearings, seals, power-conversion systems, moorings and foundations, power-export cables, pitch-motors and blades (Equimar[3] and RealTide[4]). In addition, *normal* operating conditions and their aggregated long-term effects must be considered to ensure adequate fatigue life of components. However, there are a lot of uncertainties regarding both the characterization of realistic environmental conditions and the impact of such conditions on the loads induced on the turbine. These uncertainties can lead to unexpected failures if the loads are underestimated or increased costs if the security factors used in design are too high.

The simplistic view for computing energy extraction from a tidal site [5] is to determine the tidal variation in the flow at a given point in space, convert this to an estimate of available kinetic energy, then convert this to power extraction via an efficiency factor for the turbine. This can be integrated over a single tidal cycle, or over a full year to capture the effects of annual variability. Similar approximations can be made to the loads, by estimating the force applied to blades and the variation of this over multiple tidal cycles. This approach throws away all of the higher frequency variability inherent in high-energy tidal sites, does not take into account the effects of waves, and often misses the impact of locally generated flow structures that may be missing from *in situ* measurements and low-resolution numerical models of the tidal flow.

The presence of the higher frequency processes can significantly modify the estimates of available energy, and may also impact on estimates of a turbines mechanical efficiency. In terms of turbine loads, it has been shown that waves and large scale coherent turbulent structures have a significant impact. The frequencies associated with these physical process need to be considered when designing a blade that has sufficient resilience to survive for extended periods in the harsh marine environment. These vibrational modes will be transferred to the mechanical conversion systems of the turbine, and thereby increase the fatigue cycles of these components, reducing turbine reliability.

There are also uncertainties regarding the estimation of the loads induced by such environmental conditions. Numerical models are often used to predict the turbine loads and performances at the design stage. Model outputs will help specify turbine components and estimate system power production. As measuring the loads applied on a turbine deployed at sea is complex and expensive, there is currently a lack of publicly available knowledge on the actual loads induced on a turbine and therefore limited feedback on the accuracy of load prediction by numerical models.

In order to understand the behaviour of tidal turbines operating under realistic environment conditions many different numerical techniques have been implemented. In the work of [6] numerical approaches regarding turbulence models, wall functions, meshing, as well as transient and steady solutions were conducted for a 2-bladed tidal turbine with a blade resolved Computational Fluid Dynamics (CFD) model. They recommend the use of a steady moving reference frame and k-w SST with wall-function to balance accuracy and computational effort. Using a Blade Element Momentum Theory (BEMT) model [7], carried out a sensitivity analysis of inflow parameters, geometrical design, and operational condition, including current and waves, on the load response of a tidal turbine. They found that off-axis loads on the shaft were considerable influenced by the rotor out-of-plane bending moment, and they reported that situation as significant for the majority of their tests. The Wind and Tidal Turbine Embedded Simulator (WATTES) was presented in [8]. It simulates a wind turbine rotor, based on BEMT, into a Large-Eddy Simulation (LES) CFD solver. The CFD solver uses an adaptive mesh to increase and decrease the mesh resolution. However, the CFD solver used by WATTES is under limited support. A comparison of numerical approaches for the simulation of tidal turbines was presented in [9]. They considered the BEMT, blade element actuator disk (ADM), ADM-CFD (using RANS), blade-resolved CFD (using moving reference frame), and coastal models (using shallow water correlations). They reported congruity in results for ADM-CFD and a coastal area model for a headland case using a simplified turbine fence. In [10] (using field and TEC data from the ReDAPT project) a very high resolution simulation featuring both RANS and LES turbulence implementations was carried out. Good agreement was found between methods for low levels of turbulence with the LES method additionally resolving blade-generated turbulence, however, due to computational cost (the simulations were run on EDF's Blue Gene Q supercomputer) only a limited number of inflow cases could be modelled and waves were not included.

1.1 RealTide Project

The RealTide project (www.realtide.eu) aims to improve turbine reliability by targeting uncertainties around characterisation of the marine environment together with the response of multiple sub-systems to these dynamic and energetic conditions. Three numerical models - featuring large differences in levels of complexity and computational requirements - have been used within this project to predict turbine performances and loads.

The data underlying these analyses, together with data from multiple other related simulations and tank-tests, will be made available publicly via the under-construction RealTide database. It is hoped that this database, comprising results from field, numerical and physical experiments will serve as a useful tool for model development, validation and cross-comparisons.

The aim of this paper is to assess the ability of the numerical models used in the RealTide project to represent complex realistic flow conditions and to predict the turbine response to these conditions. It aims to provide enough information to help designers to choose the numerical construct that is best suited for the situation. These decisions are usually impaired by the lack of data outlining the comparative performance and numerical costs of these numerical constructs.

The numerical models are presented in a general overview before describing how the realistic flow and the turbine were implemented in each model. The turbine response predicted by the numerical models for two flow conditions (with and without waves) is then compared to observations made during tank tests for two different turbines: one based on a commercial prototype machine and the other based on a generic 3-bladed horizontal axis turbine (HAT) design. Finally, the numerical costs of these models are compared in order to help choose the best suited tool depending on the time available and the required outputs.

2 Overview of the three numerical implementations: BEMT, BEMT-CFD and Blade-Resolved CFD

Numerical models, in the context of tidal energy, are tools used to simulate the interaction between a representation of the fluid environment and a representation of the operating tidal turbine. This can be achieved at varying levels of complexity; with more complexity typically resulting in more time-consuming and expensive simulations. Essentially, this comes down to how the physics of flow in a fluid is represented and solved and how the energy extraction process is integrated. For faster estimates of the performance, simplistic models that are based on elementary physical principles are used. If an accurate representation of the complex flow phenomenon is required, numerical models that solve the discretized Navier-Stokes equation may be used.

The numerical model constructs used for this comparative study, in increasing order of complexity, are - Blade Element Momentum Theory (BEMT), BEMT-CFD coupled simulations and blade resolved Reynolds Averaged Navier-Stokes (RANS) equations based CFD simulations. This section gives a brief overview of the models used.

2.1 StarBlades - BEMT

Blade Element Momentum Theory (BEMT) provides the most simplified numerical model of the tidal turbine [11], based on classical laws of physics such as Newton's Laws of Motion and conservation of momentum. The flow modification by the rotating turbine is modelled in terms of axial and tangential induction factors. The axial induction factor represents the change in the magnitude of axial velocity in the flow, while passing through the turbine; the tangential induction factor represents the same for the tangential velocity component. These induction factors are then computed by applying the principles of conservation of linear and angular momentum.

StarBlades - a BEMT tool for realistic flow conditions - was developed under Task 3.1 of the RealTide project, based on these concepts [12]. To improve on the assumptions and limitations of classical BEMT, improvement modules were included within this code, following the work by Scarlett & Viola [13]. The objective was to obtain a simplified numerical tool capable of running on a laptop computer with relatively faster and accurate computation results.

The validation of the BEMT computations have been made with available experimental and CFD results. Being a relatively new industry, there are not many test cases available within the tidal turbine industry, especially for dynamic analysis. However, the BEMT is also applied for wind turbines, where the fluid environment changes but the fluid mechanics remain the same for the operating scenario. Moreover, the amount of experimental research conducted in the aerodynamic industry, particularly for wind turbines, is larger. Many commercial tidal turbine codes have used wind turbine data for validation. Hence, the use of such data was also considered in the validation process. The results from the validation study are presented in the public deliverable D3.1 [14].

2.2 SOWFA - BEMT-CFD

SOWFA [15] is a open-source CFD simulator for wind turbines applications. The turbine model of SOWFA uses BEMT together with an Actuator Line Model (ALM) [16] to calculate the body force exerted on the fluid as a response of the hydrodynamics forces applied to the blades. In SOWFA, the turbine model, implemented entirely in C++, is embedded within an OpenFOAM toolbox [17]. Turbulence in the flow is modelled using a Large Eddie Simulation (LES) approach [18]. Although originally implemented for wind turbines, the fastFlume model allows tidal turbines to be simulated [19]. As SOWFA is an open-source under continuous development and support (nwtc.nrel.gov/SOWFA) and because its CFD solver is the recognized OpenFOAM toolbox, it was decided to use SOWFA in the development of this work. The version of SOWFA used in the present work does not consider either the rotor hub or the turbine support structure.

For the simulation of the ocean environment, OpenFOAM solves the incompressible continuity equation and Navier-Stoke equations. Large scale turbulent structures are solved while small scale turbulence is accounted for using an LES sub-grid scale model. The governing conservation equations are solved using an unstructured, collocated, second-order, Finite Volume Method (FVM). The implicit pressure coupling needed by incompressible solvers is obtained using the pressure-implicit splitting operation (PISO) algorithm with three sub-step corrections [20].

The interaction between the turbine rotor and the ocean environment is managed as follows. In the ALM the velocity field in the rotor plane is used to calculate the lift and drag forces acting on each turbine blade. The total forces exerted on the rotor is then used to calculate the net torque and thrust. At the same time the body force exerted on the fluid by each blade element is calculated and projected onto the control volumes in the rotor plane.

The calibration of a particular tidal turbine model is carried out according to a thermodynamic energy balance criterion. The body force spreading is used to regulate the energy balance. If the projected body force is reduced, it means that less energy is dissipated to the environment and more kinetic energy is captured by the tidal turbine. Similarity, if the body forces are reduced, the flow around the tidal turbine will be more stable with less wake generation.

2.3 STAR-CCM+ - Blade-Resolved CFD

Blade-Resolved CFD provides one of the most detailed numerical model available to simulate the operation of tidal turbines in realistic conditions. It is the only one of the three models considered that takes into account an accurate description of the geometry. A mesh is used to discretise the associated 3D CAD and implement it in the numerical model. Thanks to this, the turbine rotation is resolved accurately enabling a good capture of the hydrodynamics. It enables to quantify the efficiency of the turbine in various inflow conditions. However, this model also asks for a fine mesh of the domain to integrate the inflow conditions and the wake resolution. These specificities generate a very high computational costs necessary to run it. As such, long simulations are difficult to carry out.

The Blade-Resolved CFD model considered hereafter has been developed and calibrated in the Task 3.2 of RealTide project [21]. The numerical model integrates a simplified free surface and is based on the RANSE method. It limits the possibilities for accurate turbulence resolution or realistic wave integration but enables a reasonable CPU cost.

The calibration of the model has been done using an iterative approach. It is fully presented in public deliverable D3.2 of RealTide project [21]. At first, a simplified model based on reference frame motion (RFM) was developed. Multiple sensitivity analysis were carried out to quantify the influence of the mesh, time step, simulation duration. This model was used to calculate performance curves of D10 and D12 Sabella's turbine along with Edinburgh generic turbine. Results were compared to experimental data showing satisfying agreement. Secondly, the model was further developed to integrate sea bottom, realistic inflow conditions such as vertical velocity profiles, turbine structures and simplified waves. It was necessary to change rotation method from RFM to rigid body motion (RBM). Once again, various tests were carried out to quantify the influence of boundary conditions and domain size and get the most coherent model setup. Finally, the Blade-Resolved CFD model was used to simulate realistic operating conditions of the D12 turbine on the Fromveur site.

3 Flow representation

The main objective of this work is to provide an inter-comparison between the different approaches to modelling tidal turbines alongside detailed experimental studies. To achieve this, it is important to target and replicate accurate representations of the inflow conditions based on real-world conditions, whilst recognising tank-test capabilities and numerical simulation treatment of these inputs. Tidal sites inherently have very complex tidal flow fields that vary significantly over short spatial and temporal scales, which impose dynamic and varying loads on tidal turbines ([22]). The underlying 3-D turbulence results from the very strong vertical and horizontal

velocity shear generated through boundary friction. There is the added complication that the majority of the identified tidal energy extraction sites are also exposed to wind generated waves and open-ocean swell.

3.1 Flow decomposition

The complex tidal environment is thus treated as a summation of multiple underlying processes. This leads to a decomposed description of the velocity field. This section discusses this decomposition, and provides a comparative study of the inflow conditions used in the different tools.

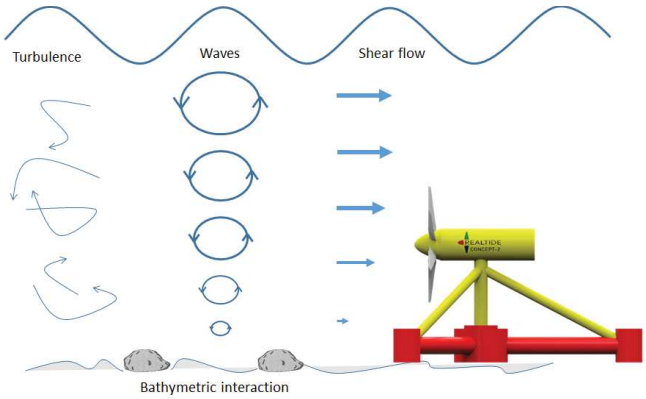

Figure 1: Factors causing non-uniformity in the flow field around a tidal turbine, after Myers [23].

3.1.1 General description of flow

The generic form of the inflow condition that will be used for the analysis can be written as:

$$\vec{U}(\vec{x},t) = \langle \vec{U}(\vec{x},t) \rangle + \vec{u}_{orb}(\vec{x},t) + \vec{u}_{trb}(\vec{x},t) \pm \sigma_{\vec{U}} \tag{1}$$

where $\langle \vec{U}(\vec{x},t) \rangle$ is the mean flow vector, $\vec{u}_{orb}(\vec{x},t)$ is the wave orital velocity, $\vec{u}_{trb}(\vec{x},t)$ is the turbulence, and $\sigma_{\vec{U}}$ is the associated uncertainty for a given measurement of the flow. The vector $\vec{x}$ defines the spatial location of the velocity measure and t is time.

Point measurements of the flow condition are collected as part of the experiments. Time series of these measurements have been used to construct suitable inflow conditions for the numerical simulations. The model domains used for the numerical simulations are simplified channels where it is assumed that the across-channel velocity is homogeneous, with an imposed vertical shear profile that represents the presence of a near-bed friction-driven turbulent boundary layer, *i.e.* $\langle \vec{U}(\vec{x},t) \rangle = \bar{U}(z)$. Waves are modeled as long-crested harmonic plane waves propagating along the channel, *i.e.* $\vec{u}_{orb}(\vec{x},t) = u_{orb}(z,t)$. Based on the tank conditions, a vertical profile of the wave orbital velocities can be calculated using linear theory. The implementation of turbulence is problematic for the numerical models being used since $\vec{u}_{trb}$ varies significantly in time and space. Consequently, we attempt to include turbulence based on the experimentally observed turbulence intensity (TI). The method for implementing the inflow conditions will be outline in this section, along with a description of the model domains used and the corresponding controls on the simulated turbine response.

3.1.2 Mean flow shear profile

The simplest inflow condition is a constant mean flow, but to be representative, the vertical shear profile that results from friction with the bottom of the channel must be included. For open channel flows, it has been shown [24] that the shear profile follows a simple power law. The power law shear profile is a function of height above bottom (z), and assumes a no-slip boundary condition at the bottom of the basin, with the flow strength increasing with towards the fluid surface. The reference velocity (U_{ref}) at a known height (z_{ref}) is defined as:

$$\bar{U}(z) = U_{ref}(\frac{z}{z_{ref}})^{\frac{1}{n}} \tag{2}$$

The power law coefficient for the FloWave basin [25] has been shown to be $n = 15$. Since the IFREMER facility has a similar profile, $n = 15$ is used for both. The corresponding current velocity profile is shown in Figure 2 for a reference velocity of 0.8 ms^{-1} taken at the hub centre, in the rotor plane.

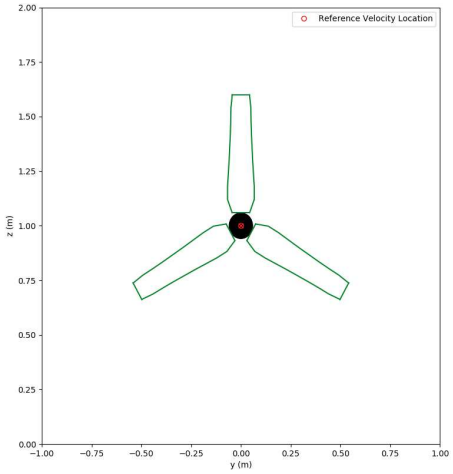

(a) Location of the reference velocity measurement

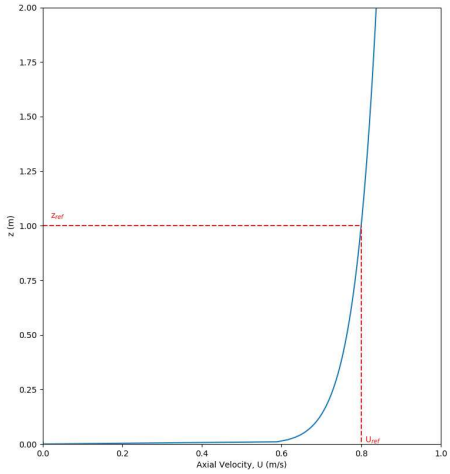

(b) Simulated vertical current velocity profile with $n = 15$

Figure 2: Illustration of the current velocity profile for a reference velocity of U = 0.8m/s at hub height and a power law factor n = 15

3.1.3 Wave Implementation

Wave energy propagates by displacement of the free surface, with an exponential decay in wave forcing with depth below the surface. The fluid particles at a given point the water column move in an orbital motion in the vertical plane parallel to the waves propagation direction, *i.e.* there is horizontal and vertical component of velocity due to the wave orbital motion. The wave energy propagates in the wave direction at the waves phase speed, which will generally be different to the underlying fluid flow speed. The interaction between the wave and fluid flow needs to be accounted for when defining the wave inflow conditions. The main obstacle in introducing waves into the numerical simulations is that none of the constructs consider in this work have a free-surface or a method for driving waves into the model domain. This limits the investigation of wave-machine interactions to following waves, *i.e.* waves travelling in the same direction as and parallel to the flow.

The method proposed for simulating the wave as an inflow condition is to consider only the horizontal component of the wave orbital velocity and its variation with depth. This velocity component will be added to the mean inflow described in Section 3.1.2, giving:

$$U(z,t) = \bar{U}(z) + u_{orb}(z,t) \tag{3}$$

For a harmonic plane wave following a fluid flow, the wave form will change through a Doppler shift in the apparent wave frequency relative to a given fixed point in space, *i.e.* the wave propagates in a moving reference frame. This change in frequency has a corresponding change in wave amplitude, and wave orbital velocities. The Doppler shifted relative wave angular velocity is given by $\omega_r = \omega + k_r U$. The modification to the wave form can be approximated using linear wave theory [26], through the Doppler shifted dispersion equation:

$$\omega + k_r \bar{U} = \sqrt{g k_r \tanh k_r d} \tag{4}$$

where $\omega = 2\pi f = 2\pi/T$, k_r is the relative wave number, g is the gravitational acceleration, and h is the water depth. The transcendental dispersion equation (4) needs to be solved numerically to obtain k_r.

The horizontal component of the relative wave orbital velocity is given by:

$$u_{orb}(z,t) = a\omega_r \frac{\cosh(k_r z)}{\sinh(k_r h)} \sin(\omega_r t + \phi) \tag{5}$$

where a is the wave amplitude, z is the depth below the fluid surface (-ve downwards), and ϕ is the phase lag in the wave at the open boundary. Substituting equations (5) and (2) into equation (3) gives the mathematical form for the inflow condition of waves + fluid flow:

$$U(z,t) = U_{ref}(\frac{z}{z_{ref}})^{\frac{1}{n}} + a\omega \frac{\cosh kz}{\sinh kd} \sin \omega t \tag{6}$$

3.1.4 Turbulence Implementation

In depth constrained flow environments (where the water depth is much less than the horizontal spatial scales), turbulence is characterised by both large scale coherent structures (such as eddies), and the corresponding

energy cascade at length scales less than the water depth, that leads to the viscous dissipation of the shear generated turbulent fluctuations in the fluid flow. The large scale coherent structures are formed through an 2-D turbulence enstrophy cascade [27] caused by vertical and horizontal constraints of the fluid flow by the local topography. These large-scale coherent turbulent structures will have length scales comparable to the rotor diameter, particularly in cases where the rotor covers a significant proportion of the water depth. The shear in the velocity associated with these fluid structures are likely to have a significant impact on the turbines behaviour. Most numerical solvers for the Navier-Stokes equations of fluid motion will include a model for sub-grid scale turbulence closure, but in the absence of boundary friction or flow separation points within the domain, large scale turbulent structures will not form. The numerical simulations need to be able to capture these coherent structure in a way that is representative of those observed in the tank experiments.

Within the tidal sector, it is common practice [22] to represent the level of turbulence using the turbulence intensity (TI) factor. This is a non-dimensional measure of the magnitude of velocity fluctuations in relation to the mean velocity along one of the flow axes. Turbulence intensity values at tidal energy sites are highly dependent on flow speed, tidal phase, and depth [28]. To calculate turbulence intensity, here denoted as TI_x for stream-wise flow, the standard deviation of the velocity fluctuations along the desired axis is divided by the mean velocity of the bulk inflow, $\overline{U}$:

$$TI_x = \frac{\sigma_x}{\overline{U_x}} \tag{7}$$

where the standard deviation σ_x is the square root of the variance:

$$\sigma = \sqrt{\frac{1}{N}\sum_{n=1}^{N}\left(u_n - \overline{U}\right)^2} \tag{8}$$

where u_n is a discreet instantaneous velocity measurement in the stream-wise flow direction and $\overline{U}$ is the mean value over a defined period of stationarity.

3.2 Flow implementation in the models

Measurements of fluid velocity and surface elevation collected during tank testing are used to parameterise the inflow conditions for numerical simulations. The conditions are chosen to be representative of full-scale sites whilst being able to be replicated within the operating limits of the test tank facilities. Where possible common definitions of the open boundary conditions have been applied, allowing an investigation of the causes of observed differences between model results. The tank data being used are from two very different test facility setups. The IFREMER tank, where the D12 model was tested, is a linear recirculating flume, with the capability to drive monochromatic surface waves either following or opposing the flow (see Figure 3). The FloWave basin, shown in schematic form in Figure 4, used to test the Generic model, is a circular recirculating tank, with the capability to drive waves of varying spectral complexity in any direction relative to the flow. It enables to replicate a wide range of environmental conditions. A summary of the physical scale modelling used in the analysis is provided in Section 3.2.1.

3.2.1 Tank tests

The test basin at the FloWave Ocean Energy Research Facility was used to test the Edinburgh generic 3-bladed turbine model. The water depth is 2m and the circular tank is 20m in diameter. The flow can be driven from any arbitrary direction through the use of the numerous separated impellers around the basin (*i.e.* 360/28 = 12.9°). The flow is shaped by controlling the speed of the across-flow impellers. The maximum flow speed for the tank is 1.2m/s, this is limited by the stability of the wavemaker paddles which respond to the flow. The level of turbulence in the basin cannot be controlled, it is a function of the impeller driven flow and the flow conditioning filters [29] that surrounds the test floor within the basin. Through accurate control of the array of wavemaker paddles, waves of any spectral form and direction can be programmed. This allows a wide range of wave-current interaction conditions to be simulated.

Included in the data available from the tests are a series of flow-only runs where the target mean fluid speed was 0.8m/s (with corresponding TI values of approximately 7 %), and the tip speed ratio (TSR) was varied from 3.0 to 13. The optimal operating TSR for the generic turbines was shown to be 7.0 [30]. The number of these test cases that each model type can reproduce depends on their individual computing requirements, *i.e.* not all test cases will be run by all three simulation types. Only one flow+wave condition will be considered in this comparative analysis, namely a monocromatic wave following the flow. This is because the numerical simulations used here are limited in how they represent waves (*i.e.* they cannot simulate opposing waves or waves at an angle to the flow), and the IFREMER tank can only simulate following or opposing monochromatic waves.

The IFREMER wave and flume tank was used to test Sabella D12 turbine. Its working section is 4m wide over 18m long and has a depth of 2m. Two pumps located under the working section are able to drive the water at a maximum velocity of 2.2m/s. Wave can be superimposed to the current using a dedicated wave-maker and turbulence intensity can be adjusted to 1.3, 5 or 15% depending on the type of flow straightener used. A detailed description of the facility can be found in [31]. The data used in this paper were obtained for a target mean flow speed of 0.8m/s and a turbulence intensity of 1.3%.

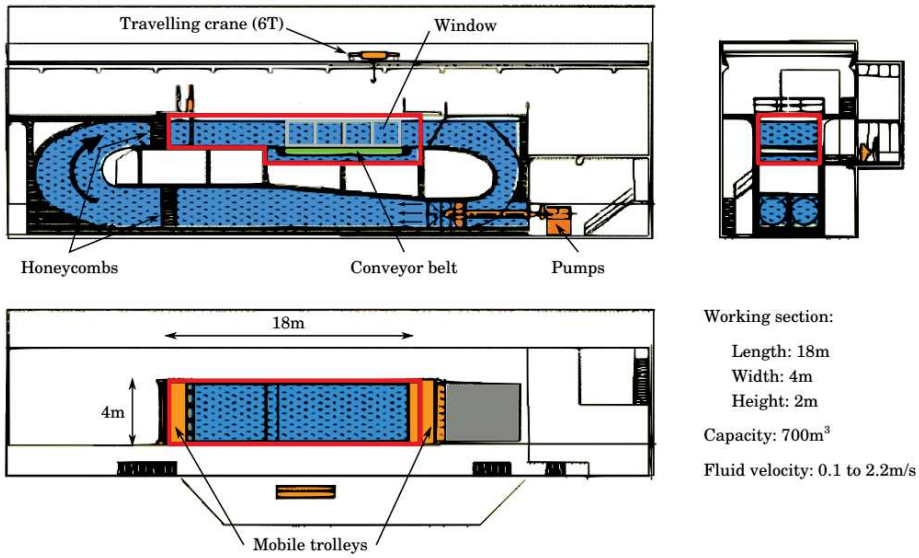

Figure 3: Schematic cross-section of the IFREMER wave and flume tank

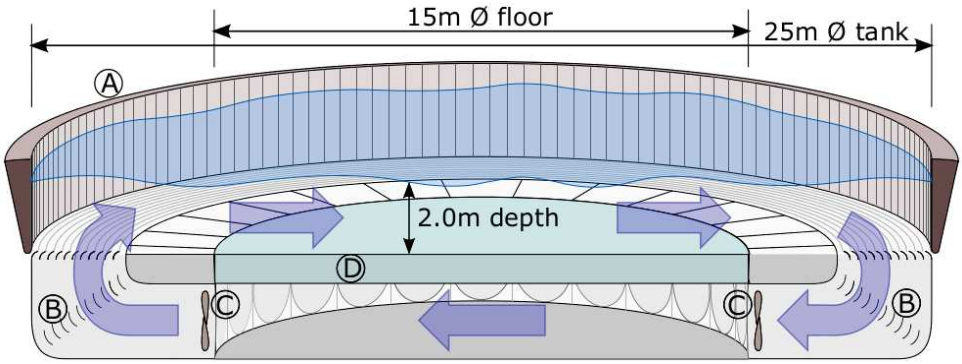

Figure 4: Schematic cross-section of the FloWave Ocean Energy Research Facility 25m diameter test basin. The water depth is 2m over the test area in the centre of the tank. The indicated components are: (A) wave-maker paddles (×168), (B) turning vanes and flow conditioning filters, (C) flow drive impeller units (×28), (D) buoyant raiseable test area floor (15m diameter).

Table 1: Test cases available for the Edinburgh generic and Sabella D12 turbines

Test cases	Parameter	Edinburgh turbine	D12 turbine
Flow only	U_∞ (m s^{-1})	0.8	0.82
	TI (%)	8.0	1.5
	TSR	3 - 13	0 - 6
Flow + waves	U_∞ (m s^{-1})	0.8	0.8
	A (m)	0.05	0.0475
	T (s)	3.33	2
	TSR	7	0 - 5

3.2.2 BEMT

The flow domain considered for the BEMT computations is a 2D rectangular plane at the rotor axis. The size of the domain corresponds to the tank width and tank height. For the comparison case studies, these values are set as 1m and 2m respectively, in accordance with the FloWave tank testing facility. The centre of the hub of the turbine located at 1m from the bottom of the tank. The discretization of the domain with a spacing of 0.01m - these are the points at which the flow environment velocity is calculated.

The StarBlades BEMT tool has the capability to include a user-defined power law for the computation of the current velocity profile along the depth of the domain [12]. For both the flow-only case and the cases with tidal currents and waves, a power law factor of 1/15 is used.

For the temporal simulations, at each instant of time, the velocity profile within the domain depth is taken according to equation 6. The velocity profile within the domain is reinitialised for each time step. These temporal simulations are performed with the velocity input from the experimental ADV sensor data. For the Edinburgh turbine, the input data is provided with a time step of 0.01 seconds (frequency of 100Hz); and for the Sabella D12 turbine, a time step of 0.0085 seconds (frequency of 117.6Hz).

While processing the velocity input from the sensor data, it is to be noted that the velocity sensor is placed upstream of the rotor plane. The location of the ADV sensors with respect to the rotor, for both experimental cases, are shown in Figure 5. For the test case where waves are included, the wave signal will propagate at the wave phase speed (c_{phase}). To recreate the response at the rotor plane a time lag ($\Delta t = x/c_{phase}$; x is distance of ADV from rotor) must be applied to the data. The phase velocity is defined as:

$$c_{phase} = \frac{\omega_r}{k_r} \tag{9}$$

where ω_r is the Doppler shifted angular frequency of the wave and k_r is the corresponding wave number, as described in Section 3.1.3. For the flow only cases it is not necessary to apply a time lag correction as the main velocity fluctuations are statistical.

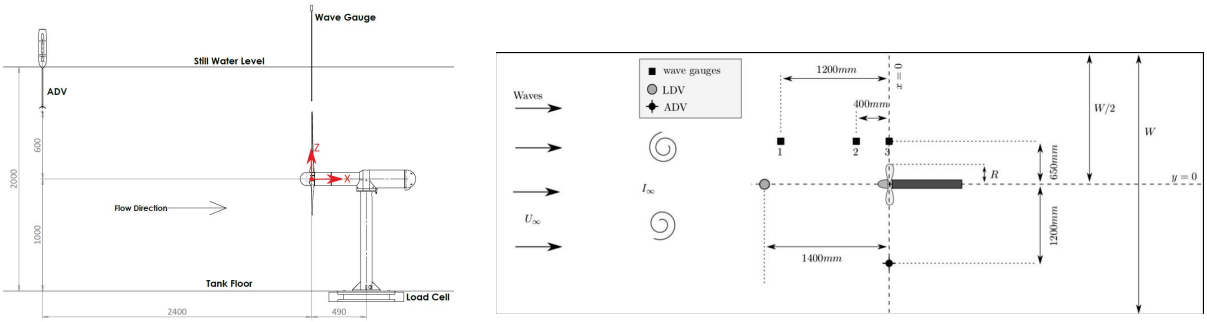

(a) Edinburgh turbine test configuration

(b) Sabella D12 turbine test configuration

Figure 5: Sensor locations for experimental testing

The magnitude of the blade forces on a quasi-static BEMT simulation varies with the square of the inflow velocity. For this reason, the high frequency fluctuations in the inflow velocity field caused by the turbulent structures significantly affect the magnitude of the output. For the flow-only simulations, there is no turbulence introduced in the model. It is important to note, however, that the driving ADV signal still contains the 7 % TI fluctuations around the mean velocity.

For the simulations with the wave input, the inflow velocity signal is obtained from the velocity sensor measurements. For these cases, the high frequency turbulent fluctuations are filtered out using a low-pass Butterworth filter of order 5 and cutoff frequency of 5 Hz.

3.2.3 BEMT-CFD

The tank environment is considered as a rectangular domain as shown in Figure 6. A velocity field is imposed at the inlet. At the outlet, the flow is considered fully developed and a zero gradient boundary condition is imposed. The top and side boundaries are considered as symmetry planes and a slip wall boundary condition is imposed. At the bottom, the flow is considered at rest (seabed) and consequently a zero flow velocity is imposed. For the simulations of the Edinburgh turbine under current only conditions (i.e. without waves) the seabed was also modelled as a slip wall.

The dimensions of the domain are as follows. For the Edinburgh turbine, a length of 10.8 m downstream is considered in order to have enough space for flow development. The water depth is 2 m (the same as that in

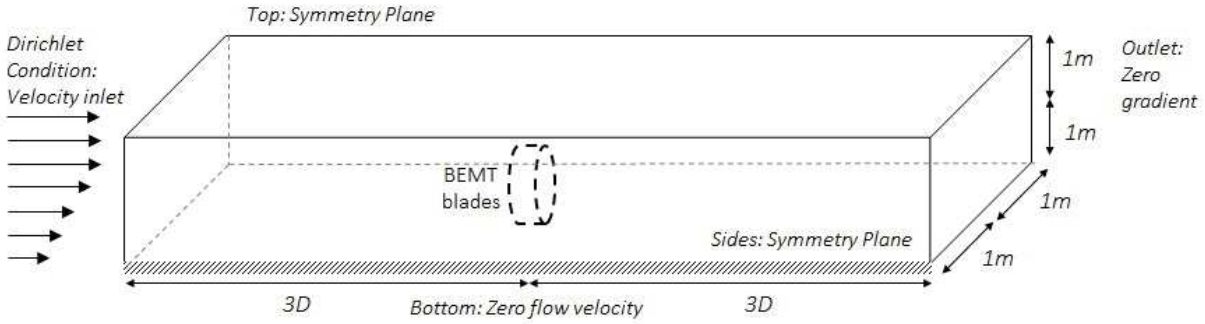

Figure 6: Domain used for BEMT-CFD model illustrated on D12 turbine

FloWave facility). The width of the computational domain (in the cross flow direction) is 4 m. This distance is considered sufficient to avoid the influence of the boundaries whilst ensuring computational efficiency. A uniform mesh distribution is used, with a cell size of 0.018 m in all directions. Similarly, for the Sabella D12 turbine, the lengths of the domain are 3.6 m, 2 m, and 2 m in x, y, z coordinates respectively, with a cell size of 0.009 m. The selected grid sizes follow the recommendations for ALM in LES simulations which are described in Section 4.3. In both cases the rotor plane of the tidal turbine is located at 3 diameters downstream from the inlet.

Measured input data files were delivered from Edinburgh generic and Sabella D12 tanks tests. They are time-series of velocity fields. At inlet, see Figure 6, the stream-wise component of the time-series is used as the reference velocity U_{ref} (see equation 2). The transverse velocity components are neglected. Consequently , in the flow only case, the flow conditions are uniform (but unsteady) across the inlet.

LES has been used to simulate the behaviour of the turbulent flow around the turbine [32]. Thus, the larger turbulent scales are directly modelled by the spatially filtered Navier-Stokes equations, and the effects of the remaining smaller scales are resolved using a subfilter-scale (SFS) turbulence model. The SFS viscosity is calculated using the Smagorinsky model. At the inlet, no synthetic turbulent inflow generator was used, because the turbulence is assumed to be included in the flow velocity field time-series.

For the combined flow and wave condition, the velocity profile, equation (6), is imposed at the domain inlet, Figure 6, and it is updated for each time-step. The reference velocity presented in the current component of the equation (6) is taking from measured fluid current time-series at the same TSR. The initial condition of the simulations considers fluid current flowing in the tank at the same TSR.

The time step has been set according to the Courant-Friedrichs-Lewy condition (CFL) based on the blade tip velocity u_{tip}:

$$\nu = u_{tip}\frac{\Delta t}{\Delta y} \leq 1. \tag{10}$$

where ν is the CFL number, Δt is the time step in s, and Δy is the smallest width (m) in the circumferential direction of the control volumes over which the blade tip passes. The blade tip velocity u_{tip} is calculated as:

$$u_{tip} = \Omega R \tag{11}$$

where Ω is the rotor angular speed in rad/s, and R is the rotor radius in m. Thus, if the rotational speed increase, a reduction of the time step will be necessary. The time-step used in the present simulations is $\Delta t = 0.002$ s. It should be noted that the time step, Δt, is much smaller than that used in the BEMT model because the stability required by the CFL number ν.

3.2.4 Blade-Resolved CFD

The simulation domain used for Blade-Resolved CFD simulations is a 3D rectangular parallelepiped as illustrated in Figure 7. Boundary conditions are set as follows:

- Inflow - Defined based on a Dirichlet condition as velocity inlet.
- Bottom - Defined as no-slip wall to simulate the influence of the tank bottom on the calculations.
- Top - Only the water domain is modelled in the simulations. Therefore, the top of the domain is defined as a symmetry plane. It is important to note that this rigid lid approximation of the free surface assumes that there are no surface waves.

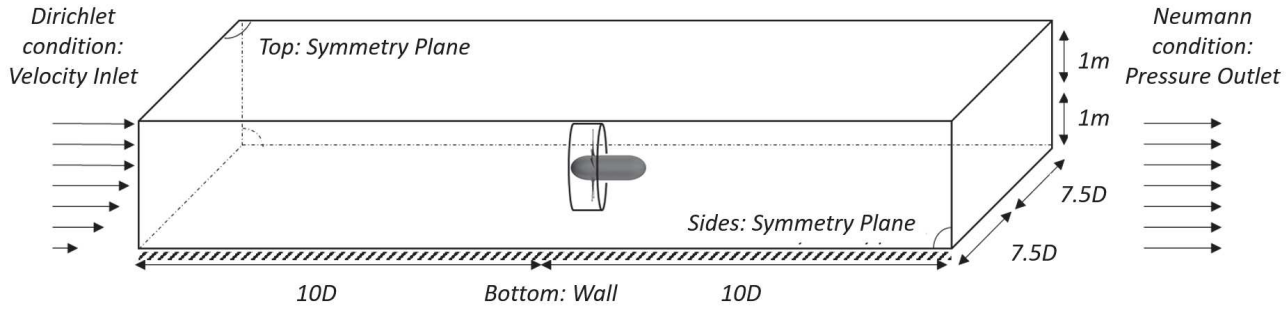

Figure 7: Domain used for Blade-Resolved CFD model illustrated on D12 turbine

- Sides - Defined as symmetry planes (walls with slip condition). Although this choice of boundary conditions normally suggests a turbine in the middle of an infinitely wide array, it is considered reasonable provide the domain is sufficiently wide.
- Outlet - Defined based on a Neumann condition as pressure outlet.

The domain height is set at 2m to reproduce the tank depth. For width and length, large distances have been chosen to avoid any influence of the boundaries on the turbine performance. They are set with respect to the turbine diameter D, the length of the domain being $20D$ and the width being $15D$. The center of the turbine rotor is located at the middle of the domain. More details on the turbine representation and control in this domain are provided in Section 4.4.

The numerical setup is based on Reynold averaged Navier-Stokes equations (RANSE) method and k-ω SST turbulence model. The turbulent intensity as well as the integral length scale of the turbulent flow are defined as parameters of the inflow condition. According to FloWave tank data, the turbulent scale has been set to 7%.

The current velocity profile introduced in equation (2) is defined as inflow condition at the velocity inlet of the domain. It generates a depth varying flow velocity that propagates along the domain. In the case where waves are modelled, the velocity profile specified at the inlet is modified from equation (2) to equation (6). In order to achieve a converging state faster, simulations with waves are started from already converged "flow only" computations at identical TSR value. A time offset is defined ensuring coherence between the previously imposed velocity profile and the new inflow including horizontal component of wave velocity.

Finally, to simulate the rotation of the turbine's rotor, the rigid body motion (RBM) method is used. To do so, the entire fluid domain has been divided in two sub-domains: one outer domain remaining stationary, one inner cylindrical domain, including the rotor, rotating on the turbine's axis. The two domain are interfaced to ensure flow continuity between them. A more detailed description of the method and detailed views of the resulting mesh can be found in RealTide public deliverable D3.2.

The time step used has been defined with regard to the rotation speed of the turbine. It enables to ensure a good capture of the flow physics independently of the case simulated. It is set such as a time step corresponds to 2 degrees of turbine's rotor rotation. A fixed number of 15 non-linear iterations are set within each time step. It corresponds to a standard value currently used as it provides a good ratio between convergence of the intermediate solution at each step and computation time.

4 Turbine representation

Two different turbine designs are being studied: (a) a generic 3-bladed HAT (built by the University of Edinburgh, UK), and (b) a $1/20^{\text{th}}$ scaled model of the Sabella D12 5-bladed concept design (built by IFREMER, France). The turbines will be referred respectively as Edinburgh generic turbine and Sabella D12 turbine. The use of the generic turbine will allow the creation of an open data set of turbine response for a range of flow conditions that can be used as test sets for tidal turbine development. The use of the Sabella D12 turbine is tied directly to the aims of the RealTide project, in particular the transfer of knowledge between the academic and commercial sector of marine tidal energy development. For commercial reasons the D12 data will be normalised, and these data will not be released with the open data set. These scaled turbines will be simulated in each of the numerical models, based on the design parameters, *i.e.* the blade length and shape, correspond drag and lift parameters, hub height and shape, and support structures. The turbine control imposed on the physical model test cases will be replicated in the numerical simulations.

4.1 Scale Model Tidal Turbines

4.1.1 Edinburgh generic model turbine

The generic turbine considered in this project was designed and built at the University of Edinburgh [30] under Phase 3 of the SuperGen programme [33]. The aim of the design criteria was to build a scaled physical model representative of a typical 3-bladed horizontal-axis tidal turbine (HAT) supported on bed-mounted tower. The design was based on the Alstom DeepGen-IV 3-bladed 1 MW HAT (rotor diameter 18m [34]). The overall configuration was optimised to allow the study of turbine loading under combined wave and turbulent flow conditions. The geometry of the scaled blades was maximized to limit the variation in blade performance with Reynolds number and represents equivalent vertical coverage of the full water depth as the full-scale machine: compared to the DeepGen-IV turbine, the model turbine is $1/15^{\text{th}}$ scale. The blade section was based on the NACA 63-8XX series, and the shape was modified at the root to facilitate hub connection.

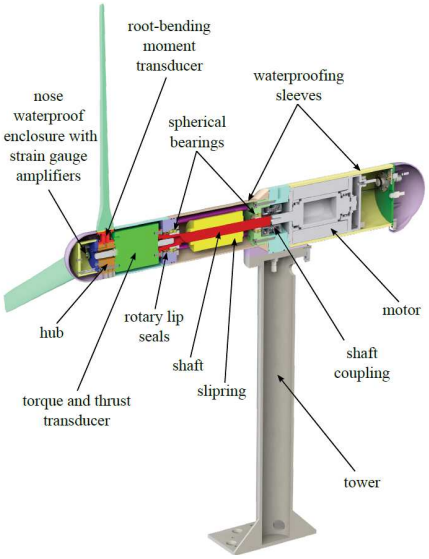

(a) Schematic of the Edinburgh generic turbine showing internal components

(b) Turbine deployed in FloWave

Figure 8: The generic 3-bladed scale model turbine built by the University of Edinburgh, UK.

The model hub-height from tank floor is 1 m, as shown in Figure 5a. Three operational parameters are measured via embedded sensors: (1) rotor thrust, (2) rotor torque, and (3) individual blade loads (stream wise root bending moment). A custom made, waterproof, thrust and torque transducer is located upstream of the shaft seal, directly behind the rotor. Custom strain gauges, located within the blade mounting system, measure the blade root bending moment. Due to space constraints these only measure the stream wise root bending moment. Turbine power-take-off is implemented via a brushless permanent-magnet servo-motor [30] selected to enable control of both speed and torque and housed within the sealed body of the nacelle. The model sub-systems are shown in Figure 9a. A range of different turbine control methods were investigated in the SuperGen tests, but the test cases considered in this paper will be limited to constant speed (or RPM) control modes. In these test cases the rotation rate is set to give the required tip speed ratio (TSR) for the chosen flow speed. This is comparable to the way in which the numerical simulations will control the turbine behaviour.

4.1.2 Sabella D12 Model Turbine

In addition to a generic HAT model turbine a commercial turbine is also considered: a scaled model (1/20th scale) of the Sabella D12 turbine. The D12 turbine is a 5-bladed tidal turbine of 12 meter-diameter with fixed symmetrical blades. The D12 scaled rotor used during tank tests was fastened on an existing IFREMER generic 3-bladed turbine which is described in detail in [35]. The hub and blades were adapted to fit Sabella D12's design (larger hub, 5 blades instead of 3). As with the Edinburgh generic turbine the D12 turbine is equipped with a waterproof thrust and torque sensor, placed directly after the rotor (e.g. before the seals). In addition, strain gauges are placed at the root of the blades supports and allow the measurement of the flap-wise and edgewise moments along with the forces applied on one blade.

Table 2: Key features of the physical models used to generate the observational data that form the basis of the numerical simulation inter-comparisons

Physical Model	Edinburgh generic	Sabella D12
Model Scale	$1/15^{th}$	$1/20^{th}$
Rotor Diameter	1.2 m	0.6 m
Hub Diameter	0.12 m	0.19 m
Hub Height	1 m	1 m
Blade Material	Aluminium Alloy (6082T6)	Carbon epoxy
Thrust Sensor	Yes	Yes
Torque Sensor	Yes	Yes
Blade Sensors	axial RBM for each blade	3 forces, axial and tangential RBM
Speed Control	Yes	Yes
Torque Control	Yes	No

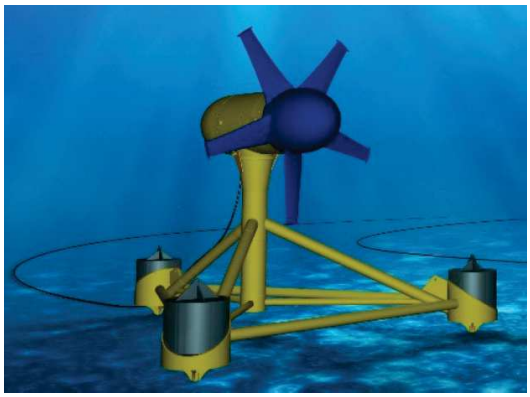

(a) Artistic view of the Sabella D12 at full scale

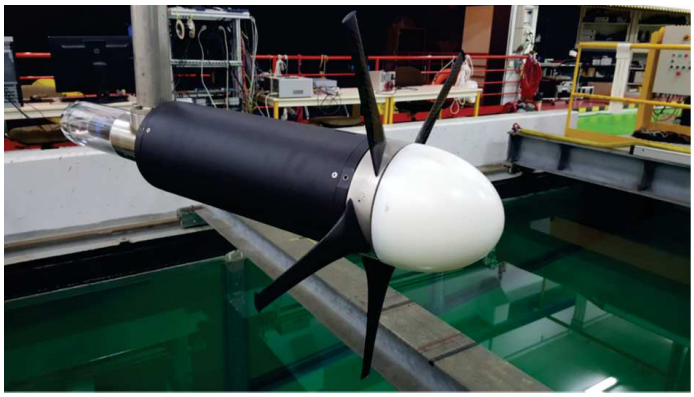

(b) Sabella D12 model scale deployed at IFREMER

Figure 9: The D12 turbine designed by Sabella, FR.

4.2 BEMT

The BEMT model includes only the blade geometry; the hub, the winglet, the nacelle and the support pillar of the turbine are not included. The blade is represented as 1D line elements, with each blade element corresponding to a foil section. The blade is discretised into 30 blade elements - 10 near the root, 10 near the tip, and 10 at the mid segment. The rotation of the turbine is simulated as an imposed, constant rotation speed corresponding to the TSR of the simulated condition.

The flow characteristics for each blade element are provided as tables of lift and drag coefficients. The generic UEDIN turbine geometry is composed of foil sections that correspond to standard NACA profiles [30]. The corresponding tables of lift and drag coefficients are obtained from [36]. The Sabella D12 blade is a hydrodynamically optimized foil geometry. The tables of lift and drag coefficients are obtained from CFD calculations.

4.3 BEMT-CFD

The model of the turbine rotor is based on the Actuator Line Model (ALM) which incorporates the Blade Element Momentum Theory (BEMT). The ALM discretizes the turbine blades as a sequence of equally spaced elements. In this work, forty elements have been used to discretize the blades of the rotor model. In each blade element, drag and lift forces are calculated according to specified aerofoil data. The aerofoil data used in the BEMT of the BEMT-CFD approach are those explained in Section 4.2. For the Sabella D12 turbine, it was assumed to be representative the aerofoil data calculated for Re number equal to one million. For this work, the rotor rotational speed is set constant over the simulation according to a determined case. The turbine model used in this work does not consider the support, hub, nacelle, and winglet.

One important part of the rotor model implemented in the BEMT-CFD approach is the manner how it calculates the body forces distribution over the actuator lines. The expression of the hydrodynamics forces projected on the flow domain [18] is presented in this equation:

$$\vec{f_{turb}} = \frac{\vec{F}}{\epsilon^3 \pi^{3/2}} e^{[-(r/\epsilon)^2]} \tag{12}$$

where $\vec{f_{turb}}$ is the projected body force per unit volume, $\vec{F}$ are the hydrodynamic forces at the blade element, and r is the distance from the centre of the blade element to the centre of the control volume. The Gaussian radius ϵ which represents the spreading of the projected forces around the blades is calculated in the model by this expression:

$$\epsilon_r = n_{max} \Delta_{grid} \sqrt{1 - (\frac{2r'}{R})^2} \tag{13}$$

where n_{max} is a dimensionless parameter to define the maximum spreading width for a given mesh spacing Δ_{grid}, a value equal to 2 was used in this work. R is the blade radius, and r' is the radius of the equivalent blade ellipse. It is recommended for ALM on LES that the relative grid spacing (Δ_{grid}/R) is approximately limited between 1/30 and 1/60 and uniform along the actuator line for using ALM and LES to model wind farms. Additionally, the relative blade element spacing (Δ_{blade}/R) is lower than 1/20 in order than the rotor thrust and power are computed accurately. This body forces approach has been developed and tested for wind turbine applications [37].

4.4 Blade-Resolved CFD

As previously introduced, Blade-Resolved CFD model provides a very realistic description of the turbine geometry. A mesh composed by millions of cells is used to discretise the associated 3D CAD and implement it in the numerical model. For this paper, calculations were carried out with only the blades (and winglets if any - cf. D12 turbine) and the hub modelled. The turbine structure has not been integrated to enable more direct comparison as other numerical models do not consider it.

The turbine control is achieved by imposing a constant and imposed rotation speed corresponding to the studied TSR. Its value is calculated based on the mean flow velocity.

Table 3: Turbine representation in numerical models

Specificities	BEMT	BEMT-CFD	Blade-Resolved CFD
Hub	No	No	Yes
Support structure	Not taken into account		
Blade representation	1D Line elements	1D Line elements	3 Dimensional
Blade discretization	30 blade elements	40 blade elements	Surface mesh composed of millions of cells
Foil performance	Table of lift and drag coefficients		Computed
Turbine control	Forced constant rotation speed throughout simulation		

5 Model inter-comparison

The purpose of the analysis presented in the section is three-fold: (1) Determine how well the numerical simulations predict the observations; (2) Determine how the definition of the inflow conditions for numerical simulations affect the performance predictions; (3) Identify the limitations of the various numerical simulation constructs. The standard method for comparing different turbines is to use the non-dimensional performance coefficients (C_P, C_T, C_Q, C_{RBM}). To address (1) we will use these performance coefficients to determine how well the various numerical simulations predict the observed turbine responses for the two physical models (Generic, D12). The hypothesis is that if the numerical simulations are correct they will return the same coefficient values. To address (2) we will compare the flow only cases with the flow+wave cases, where there is a common TSR value. The aim is to determine firstly how the presence of waves affects the turbine performance (based on the observed data), and secondly if the simplified method used to include waves in the numerical simulations is sufficient. For this analysis the predicted physical parameters (P_x, T_x, Q_x, RBM_x; x = data source) will be normalised by the mean observed parameters ($\overline{P}_{obs}$, $\overline{T}_{obs}$, $\overline{Q}_{obs}$, $\overline{RBM}_{obs}$). Finally, (3) will be addressed through an analysis of the predicted spectral response from time series of the normalised physical parameters. These will be interpreted in the context of the complexity of the various numerical simulations.

5.1 Observed test tank flow and wave conditions

When the tank test are run, target values for the flow speed are chosen, a level of TI is set by flow-conditioning, and, if waves are included, the target wave amplitude and period are defined. The achieved values for these inflow parameters will differ from the target values due to limitations in the mechanical systems to precisely reproduce the target conditions. Measurements provided by the ADV or LDV, and wave gauges are used to determine the actual flow parameters that the physical models are responding to. Any difference between the target and actual values need to be taken into account when assessing the validity of the numerical simulation predictions. The target and observed values for the comparable flow-only and and flow+wave case are given in Tables 4, 5 and 6. Some of the wave parameters are recovered from the observed data using the linear wave theory described in Section 3.1. For the observations, these have been included in a separate column in Tables 5 and 6.

The extraction of the observed flow only parameters is a straightforward deconstruction of the ADV or LDV velocity data. The process simply involves applying quality controls to the time series (unwrapping and/or despiking using phase space methods), then calculating the mean velocity, then calculating the TI using the variance of the velocity.

Table 4: Target and observed flow only parameters.

	FloWave Basin		IFREMER Flume	
Parameter	Target	Observed	Target	Observed
U_∞ (m s^{-1})	0.8	0.81 ±0.06	0.8	0.79 ±0.01
TI (%)	8	7.8	1.3	1.7

The extraction of the wave parameters is slightly more complicated. This requires both the ADV or LDV data and the corresponding wave gauge data. The velocity data are quality controlled as for the flow only case. Spectral analysis of the wave gauge data showed that there is non-linear wave interaction with the tank floor for both tanks, leading to the formation of a second order Stoke's wave. In this case energy is transferred to the first harmonic of the dominant wave period (T). This was taken into account by fitting a pair of harmonics with $f = 1/T$ and $f = 2/T$ to the time series to determine the actual wave period. The optimal wave period was found by a simple iterative search for the closest fit to the wave gauge data. The amplitude of the harmonic corresponding dominant wave period (T) gives the wave amplitude (A).

The wave orbital velocities are integral to the velocity signal measured within the ADV or LDV. The orbital velocities are driven at the wave frequency ($f = 1/T$), so the orbital velocity (u_{orb}) signal is extracted by fitting a single harmonic at this frequency to the velocity data. The reconstructed time series for the orbital velocity is subtracted from the original velocity data, leaving the mean free-stream flow (U_∞) plus the turbulence (TI).

Having obtained the key parameters for the flow and wave, linear wave theory can be used to calculate the wave orbital velocity (u_{orb}), the relative angular frequency (ω_r) and relative wave number (k_r), then the wavelength (λ), wave speed (C_{phase}) and amplitude (A) can be determined theoretically. The results are tabulated separately for the FloWave basin (Table 5) and the IFREMER flume (Table 6).

Table 5: FloWave basin target and observed flow+wave parameters

Parameter	Target	Observed	Linear Wave Theory
U_∞ (m s^{-1})	0.8	0.77 ±0.06	–
TI (%)	8.0	8.4	–
A (m)	0.05	0.064	0.068
T (s)	3.33	3.24	–
u_{orb} (m s^{-1})	0.1102	0.1479	–
ω_r (rad s^{-1})	1.576	–	1.628
k_r	0.389	–	0.404
λ (m)	16.16	–	15.55
C_{phase} (m s^{-1})	4.05	–	4.02

Table 6: IFREMER flume target and observed flow+wave parameters

Parameter	Target	Observed	Linear Wave Theory
U_∞ (m s^{-1})	0.8	0.84 ±0.09	–
TI (%)	1.3	11.1	–
A (m)	0.0475	0.0298	0.0512
T (s)	2.0	2.0	–
u_{orb} (m s^{-1})	0.0752	0.0816	–
ω_r (rad s^{-1})	2.552	–	2.532
k_r	0.737	–	0.729
λ (m)	8.52	–	8.62
C_{phase} (m s^{-1})	3.46	–	3.48

The largest impact on the analysis will be related to the difference between the target mean free-stream velocity and the observed value. The normalising factors used to define the performance coefficients (see Section 5.2) are dependent on the square or cube of the free-stream velocity. In the following analysis, the target free-stream velocity will be used to define the various normalising parameters. The difference between the target and observed free-stream values will contribute to any differences identified between the observed and predicted performance coefficients.

5.2 Non-dimensional performance coefficients

The two turbines deployed in the tank test have sensors that return the following three physical parameters: (1) the rotor thrust T, (2) the rotor torque Q, and (3) the blade root bending moment RBM. The mechanical power P is a derived from the torque using the angular frequency of the rotor. These quantities can be expressed as non-dimensional performance coefficients that are used to characterize tidal turbines: C_P, C_T, C_Q and C_{RBM}, given by the following equations:

$$C_P = \frac{P}{\frac{1}{2}\rho\pi R^2 u^3} \quad ; \quad C_T = \frac{T}{\frac{1}{2}\rho\pi R^2 u^2} \quad ; \quad C_Q = \frac{Q}{\frac{1}{2}\rho\pi R^3 u^2} \quad ; \quad C_{RBM} = \frac{RBM}{\frac{1}{n}\rho\pi R^3 u^2} \tag{14}$$

where ρ is the fluid density, R is the rotor radius, n is the number of blades, and u is the target mean free-stream velocity.

It should be noted that the use of the target mean velocity in the denominators in equation (14) - instead of the instantaneous measured value - may lead to errors on the observed and predicted coefficients and account for some of the discrepancies encountered in the results. For example, in the tank tests, for flow only cases, the difference in C_P is about ±4 % for Edinburgh generic turbine and ±3 % for Sabella D12 depending on which velocity is used for the C_P calculation. For flow + wave cases, those differences can reach ±12 % for Edinburgh generic turbine and ±15 % for Sabella D12.

As the characteristics of the commercial turbine are confidential, all results for Sabella D12 were divided by a reference value measured for a given turbulence intensity and flow velocity. Power coefficients and their standard deviations were divided by the maximum C_P value whereas other parameters and their standard deviations were divided the parameter's value at the TSR of maximum C_P. The normalised values are identified by *.

5.3 Flow-only performance coefficient

For both turbines there are a set of flow-only test data where the mean free-stream velocity is 0.8 m s^{-1}, and the TSR is varied over a range of values (Generic: 3 - 13, Sabella D12: 1 - 6). From these data the expected non-dimensional parameter coefficients can be plotted as a function of TSR. The data for the C_P are typically used to identify the optimal performance speed for the turbine. The BEMT simulation has the lowest computational overhead, so it was possible to simulate all of the available flow-only test cases for both turbines. The computational cost of the two CFD-based models limited the number of runs possible.

In this section, the measured and predicted parameters are compared for flow only conditions (e.g. without waves). The mean values of each parameters will be compared along with their variation as a function of TSR. Both statistical and spectral measures will be used to quantify the similarities and differences between the observed and numerically predicted values. The aim is to validate the numerical models ability to predict the turbine response to a given flow condition.

Tables 7 and 8 summarize the coefficients' values and their standard deviation at the TSR of maximum C_P. Standard deviations for BEMT and Blade-Resolved CFD models are not shown because they are well under one percent.

Table 7: Turbine response - Mean parameters for flow only conditions for Edinburgh generic turbine (0.8m/s)

	RPM	TSR	C_P	C_T	C_Q	C_{RBM}
Observed	90±1.4	7±1.4	0.43±0.040	0.73±0.034	0.061±0.0055	0.21
BEMT	90	7	0.41	0.86	0.060	0.25
BEMT-CFD	90	7	0.45±0.092	0.86±0.078	0.064±0.013	0.24
Blade-Resolved CFD	90	7	0.44	0.88	0.060	0.25

Table 8: Turbine response - Mean normalised parameters for flow only conditions for Sabella D12 (0.8m/s)

	RPM	TSR	C_P* (%)	C_T* (%)	C_Q* (%)	C_{RBM}* (%)
Observed (reference)	114±0.001	4.5±0.001	100±2.8	100±1	100±2.8	100
BEMT	114	4.5	96	73	97	67
BEMT-CFD	114	4.5	92±4.2	63±1.6	93±4.2	55
Blade-Resolved CFD	114	4.5	104	89	110	74

Tables 7 and 8 show that the performances of both turbines seem well predicted by the numerical models. The difference between observed and predicted values are within the uncertainty range for Edinburgh generic turbine. Figure 10 shows the evolution of the turbines' performances and loads against TSR. For Edinburgh generic turbine, the predicted C_P values lie within the uncertainty range of the tank tests for the whole range of TSR. For Sabella D12 turbine, there is a discrepancy of the Blade-Resolved CFD results at low TSR. An offset on the TSR values is visible. At model scale, Blade-Resolved CFD tends to encounter difficulties linked to the transition between laminar to turbulent regime. Hence, it is often noticed that even if thrust is usually quite correctly captured, the torque however can often be shifted or underestimated at low rotation speeds. It may explain part of the behaviour visible on Blade-Resolved CFD results. Similar results can be observed for both turbines for the torque coefficient.

The loads applied on the rotor and blades (represented by the C_P and C_{RBM}) are much less accurately predicted by the numerical models. The four bottom curves of Figure 10 shows the predicted and measured loads against TSR for both turbines. There is a reversed trend between the two turbines : the predicted loads seem well underestimated for Sabella D12 turbine compared to the observed loads but they are overestimated for Edinburgh generic turbine. Several leads have been explored in Section 5.6 to explain this difference of behaviour between the two turbines.

5.4 Response to waves

The impact of waves on tidal turbines has been observed to affect both the power generated and the mechanical loading on the blades and structure [38, 39, 40, 41]. Test with the scaled physical models of Edinburgh generic and Sabella D12 turbines have been run for a variety of scaled wave conditions. In this analysis only a single wave condition (monochromatic, following wave) has been modelled for each turbine. For both the FloWave and IFREMER tank experiments the mean free-stream flow was set to 0.8 m s^{-1}, but different wave definitions were used. For the FloWave test the wave had an amplitude $A = 0.05m$ and a period of $T = 3.33s$, while for the IFREMER test the wave had an amplitude of $A = 0.0475m$ and a period of $T = 2.0s$. These two wave cases have been simulated by the three numerical models, where the inflow condition has been constructed using the method described in Section 3.

To investigate the effect of waves on the turbine efficiency, we assume that the flow-only test case represents a simplified environmental state, with the flow+wave cases adding complexity to the inflow conditions. To compare the various parameters and the impact of adding waves, the observed mean flow-only parameters are used to normalise the both the observations and the model prediction, *e.g.* the mean power values are normalised by the mean observed flow-only power value, the thrust by the mean observed flow-only thrust, *etc.* The normalised parameters are given in Tables 9 and 10. We have not included the torque because the power is just a scaled form of the torque, so the normalised parameters are identical.

First, if we considered observed data, for Edinburgh generic turbine there is an apparent reduction in efficiency in the presence of waves, while for the Sabella D12 turbine there appears to be an increase in efficiency. However the levels of these changes are comparable to variation between the target and actual free-stream velocity achieved in the tank tests (see Section 5.2).

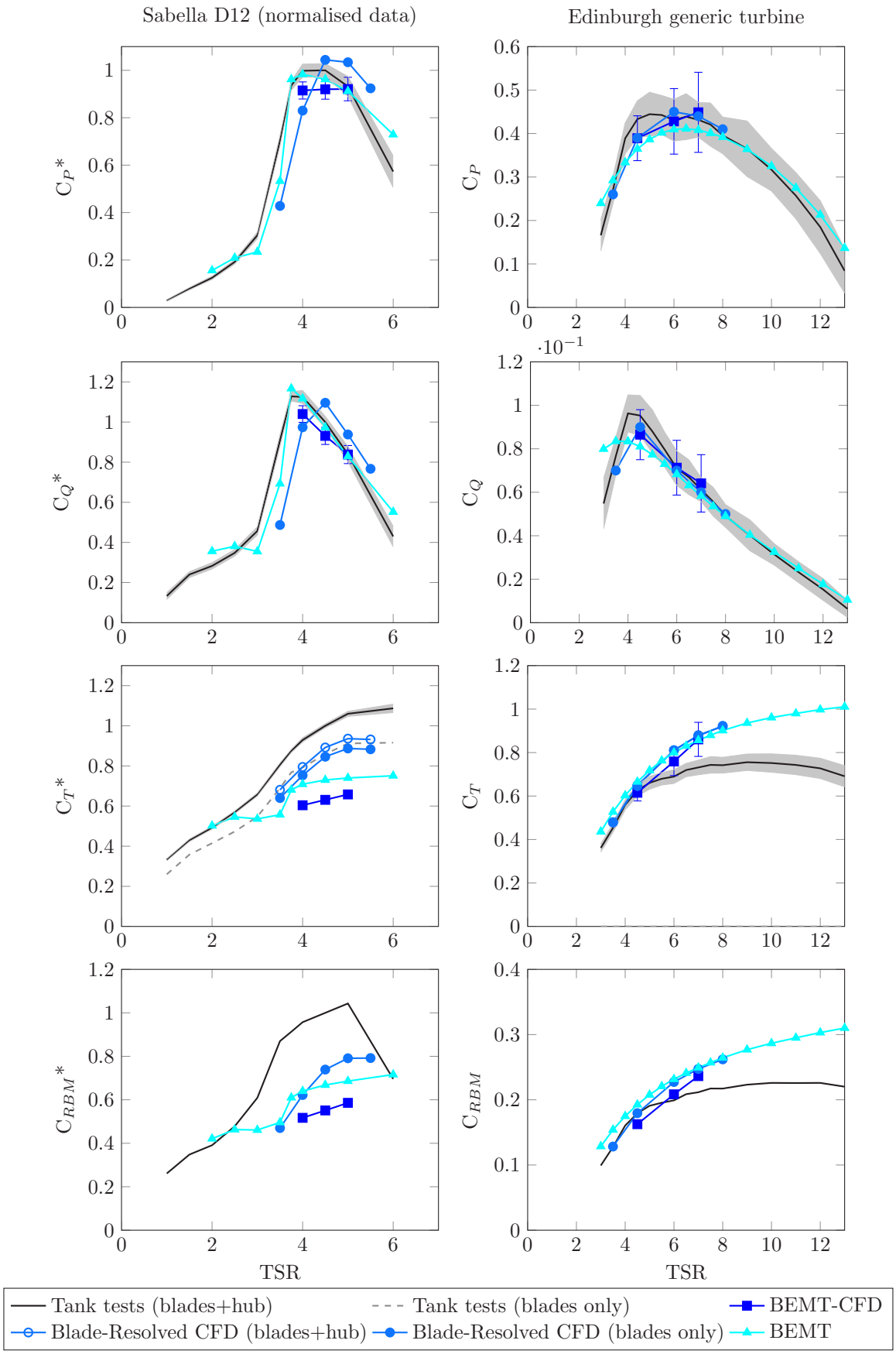

Figure 10: Measured and predicted turbine performance and loads against TSR for Sabella D12 (left, normalised data) and Edinburgh generic turbine (right) for flow only conditions

Table 9: Comparison of normalised mean physical parameters for the Edinburgh generic turbine. The normalizing factors used are the flow-only case observed values.

		Observed	BEMT	BEMT-CFD	Blade-Resolved CFD
Flow Only	P_x	100%	86%	103%	101%
	T_x	100%	111%	117%	120%
	RBM_x	100%	112%	111%	117%
Flow + Wave	P_x	88%	85%	109%	107%
	T_x	93%	111%	119%	121%
	RBM_x	93%	112%	113%	118%

Table 10: Comparison of normalised mean physical parameters for the Sabella D12 turbine. The normalizing factors used are the flow-only case observed values.

		Observed	BEMT	BEMT-CFD	Blade-Resolved CFD
Flow Only	P_x	100%	100%	97%	107%
	T_x	100%	76%	65%	86%
	RBM_x	100%	70%	55%	73%
Flow + Wave	P_x	115%	104%	98%	106%
	T_x	106%	79%	65%	86%
	RBM_x	106%	70%	55%	73%

The normalised numerical predict parameters show the same behaviour for both the flow-only and flow+wave cases. The simulations all over-predict for the Edinburgh generic turbine, and under-predict for the Sabella D12 turbine. Possible causes for the discrepancies in the simulation predictions will be discussed in Section 5.6 below.

5.5 Spectral response analysis

An analysis of the spectral response of the model predictions compared with those of the observations provides further information about the behaviour of the model, and may indicate missing processes. For this analysis, the normalisation method used in Section 5.4 will be applied to the time series. This will allow a direct comparison between the observed and predicted responses. The data are all sampled at different frequencies and are of varying lengths. To form consistent spectral forms, Welch's periodogram [42] method has been used to construct spectral density plots. A window of 2048 with 50% overlap has been used to construct all of the periodograms. This gives the same frequency spacing and a consistent spectral density estimate.

The periodograms have been generated separately for the two turbines. There is a separate plot for each physical parameters, and for the flow-only and the flow+wave cases. Figure 11 presents the results for the FloWave tests of the Edinburgh generic turbine, and Figure 12 gives those for the IFREMER tests of the Sabella D12 model scale turbine. Each plot has the observed spectral response curve overlaid with the curves for each of the model predictions. To highlight the effect of introducing the waves, a dashed version of the flow-only observed data has be overlaid on the flow+wave plots.

A consistent colour scheme has been used to various data: Observed data is blue, BEMT is orange, BEMT-CFD is magenta, and Blade-Resolved CFD yellow. The observed data (blue) are our "truth" sets that the numerical simulations are aiming to predict.

For the flow-only cases there should be peaks associated with the blade frequency in the observations from the tank tests. This is a known effect that results from the shadowing effect of the support pillar [43, 44]. The turbines are rotating at a constant RPM, so the blade frequency is given by:

$$f_{blade} = n\frac{RPM}{60} \tag{15}$$

where n is number of blades. For the Edinburgh generic flow-only tests $f_{blade} = 4.5$ Hz, and for the Sabella D12 turbine flow-only tests $f_{blade} = 9.5$ Hz. For the flow+wave cases there should also be peaks at the wave frequency. For the FlowWave generic turbine test the wave frequency is $f_{wave} = 0.3$ Hz, and for the IFREMER D12 test the wave frequency is $f_{wave} = 0.5$ Hz.

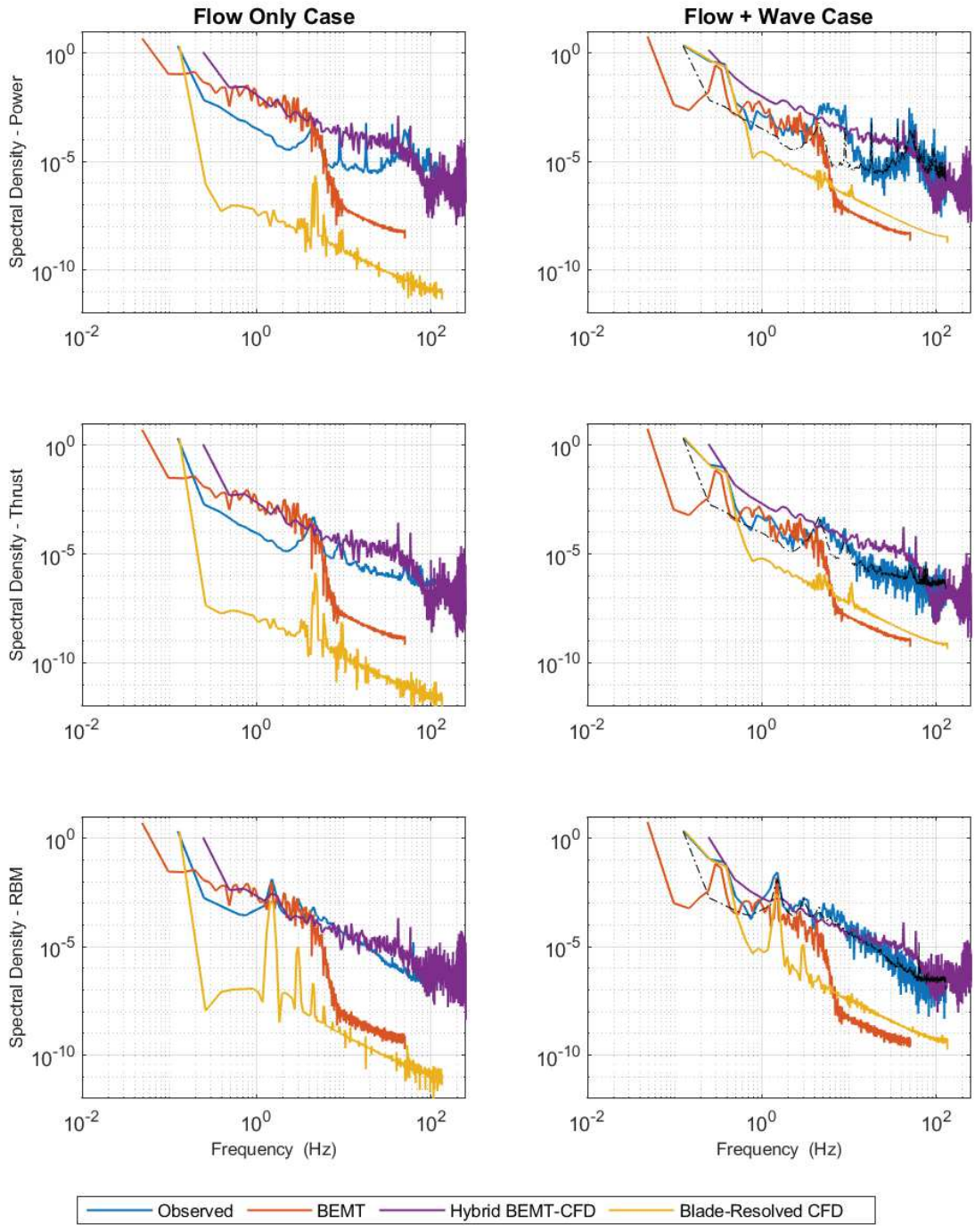

Figure 11: Normalised spectral response data for the Edinburgh Generic turbine. The three main performance parameters are present: power, thrust, and RBM. The mean of the observed parameters for the flow-only case have been used as the normalising factor. The left-hand panels are for the flow-only case: U-0.8, TSR=7.0, and the right-hand panel are corresponding flow+wave case.

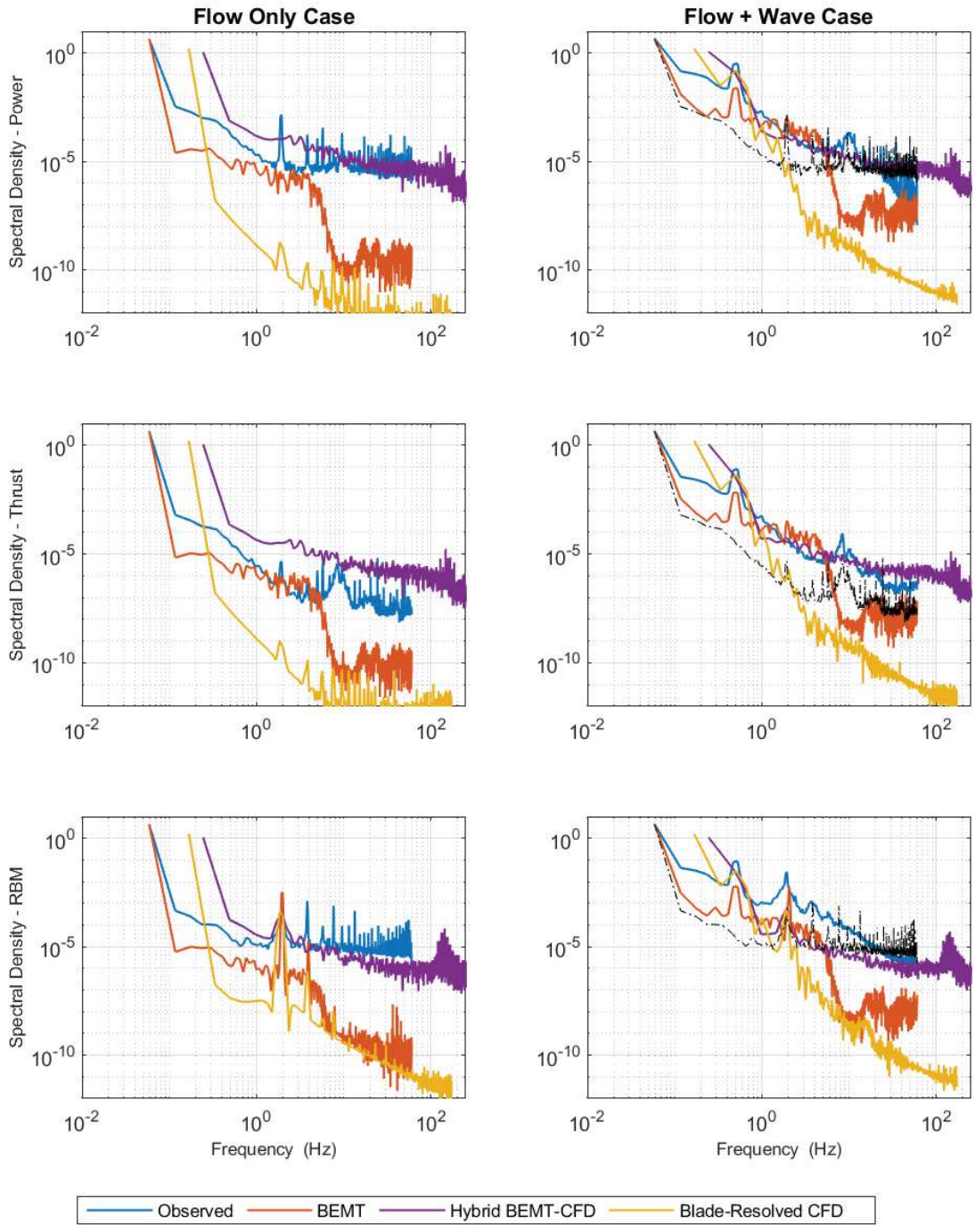

Figure 12: Normalised spectral response data for the Sabella D12 turbine. The three main performance parameters are present: power, thrust, and RBM. The mean of the observed parameters for the flow-only case have been used as the normalising factor. The left-hand panels are for the flow-only case: U-0.8, TSR=4.5, and the right-hand panel are corresponding flow+wave case.

Figure 11 collects the data for the Edinburgh generic turbine tests. Starting at the top of the figure, are the normalised power data. The observations show the distinct blade frequency spikes and higher harmonics of this peak. With the addition of the wave, there is peak at the wave frequency and a broad hump forms in the spectra from the blade frequency up to its 3rd harmonic. The remainder of the spectral form remains very similar. For the flow-only case, neither the BEMT or BEMT-CFD models capture the blade frequencies, and both have high spectral densities in the lower frequencies. The cut-off filter applied to the BEMT has its roll-off corner close to the blade frequency, so the choice of filter width is too harsh. The peak at the wave frequency is captured by the BEMT and the Blade-Resolved CFD models, but there does not appear to be a response to the wave in the BEMT-CFD model. In all cases the Blade-Resolved CFD response appears very low, this is

due to the lack of large scale turbulent structures in these simulations. It is evident from these data that it is important to capture the coherent turbulent structures when determining the spectral response to loads.

The middle panels in Figure 11 show that similar patterns are repeated for the thrust data, but the blade frequency peaks are weaker. For the RBM data (lower panels) there are two peaks below the blade frequency that are at the rotational period and its first harmonic. This effect has been identified [43, 44] as the shadowing effect on each blade through a single rotation. At the lower frequencies, the effect of the normalisation on the mean parameters can be seen. The shift up or down in frequency of the end point relative to the observations, corresponds to an over or under prediction in the mean values. These shifts correspond to the findings in Section 5.4.

Figure 12 collects the equivalent data together for the Sabella D12 turbine tests. These tests where run with a fixed turbine $RPM = 114$; for the Sabella D12 this corresponds to a blade frequency of $f_{blade} = 9.5$ Hz, and a base rotational frequency of 1.9 Hz. The wave frequency used in the flow+wave case was $f_{wave} = 2$ Hz. These are the key frequencies seen in the response spectra.

The observed response shows the blade response frequencies and the corresponding shadowing effects. In this case the lower frequency shadowing has a larger effect than the blade frequency, in contrast to the Edinburgh generic turbine. The numerical simulations do not capture the blade frequency responses in the power or the thrust, but the BEMT and Blade-Resolved CFD do appear to capture the rotational frequency response and the first harmonic. Again, the BEMT-CFD model is less sensitive.

The observed response of the Sabella D12 turbine show that the introduction of waves has a significant impact on all of the parameters. This is expected as the extra blades increases the interaction with the fluid, the 5-blade rotor of Sabella D12 turbine effectively presents a greater cross-sectional area to the flow than a 3-bladed. The BEMT and Blade-Resolved CFD simulations capture the peak wave period response, but filter out the higher frequency response seen in the observed data. The BEMT-CFD model only weakly captures the wave peak, again indicating that it does not respond significantly to the waves.

The overarching comments on this analysis are that the numerical simulations capture the parameter values in a mean sense, but have a tendency to over-estimate for increasing TSR. The simulated spectral response has been shown to be severely lacking. This suggests that the methods used in this paper are not sufficient for the prediction of load spectra. Given the significance of loading frequencies to fatigue life calculations, modifications to these numerical systems is required to better predict load spectra, in particular it is evident that the presence of the support pillar has a significant impact on the turbine response. The differences between the Blade-Resolved CFD and the other two simulation methods show that it is important to capture the large-scale coherent structures in the inflow condition. A suitable method for doing this needs to be determined.

5.6 Possible causes for discrepancies

One of the first lead investigated was the instrumentation used in tank tests. As both turbines have been tested with different instrumentation, an error in the calibration could have explained the differences between observed and predicted thrust and the fact that the turbine seem to have different behaviours. But the RBM values - measured on the blade sensor - show similar trends than those of the thrust and it seems highly unlikely that there was an error of calibration from both instruments.

The low thrust values observed for Edinburgh generic turbine might have been caused by the flexibility of the blades. Indeed the blades are long and thin and tend to flex at high TSR.

A possible explanation for the difference between observed and predicted thrust is the hub contribution as it was not included in the thrust predicted by the different models. But its contribution was estimated by Blade-Resolved CFD and found to be almost negligible for Edinburgh generic turbine (less than 1% of the total thrust). For Sabella D12, this contribution is larger (up to 6%), due to its larger diameter, but it is not enough to explain the difference between numerical models and tank test.

The low thrust values predicted by the BEMT-CFD model for the Sabella D12 can be due to the fact that the ALM calculates the force distribution along a line as it was created for slender blades like in the case for wind turbines. A correct load prediction has to consider both a radial and chord load spreading. Thus, better results of thrust were calculated for the Edinburgh generic turbine as its blades are more slender and resemble more to a wind turbine. However, for the case of the Sabella D12 turbine which has a particular geometry, bigger hub and fatter blade, the ALM and the equivalent blade ellipse were not able to calculate accurate values for the axial forces. The approach of body forces on LES is a topic of continuous researching [45] and enhanced models are expected to be used in order to improve the results.

6 Computational cost

When comparing the results obtained between experiments and various numerical models, one has to keep in mind the cost associated to each of these numerical approaches. Indeed, this parameter varies quite significantly

depending on the considered approach and it may orient the decision to prefer one to another. Therefore, this section aims at comparing it for the three methods of interest in this paper. It will enable to add context to the presented results and analyse the obtained results through a new angle. It includes the time necessary to go from the definition of the model to the post-processed data.

The time taken for each simulation technique is mentioned step-wise in Table 11 and Table 12. Table 11 indicates the time taken for the simulations with only current flow. Table 12 indicates the time taken for the simulations with current and waves. For time domain numerical simulations, the indicated time is the time taken to attain a converged solution for 30 seconds of time-series data. The values are provided based on the Edinburgh generic turbine running at TSR = 7 in order to ensure comparable information. For the flow only condition, the time presented in Table 11 is for 12 computational seconds of the BEMT-CFD model.

The time provided is only indicative and meant to provide the reader a guidance about the scale of computational effort required for each simulation technique. It may also be noted that for this comparison study, all numerical models are assumed to be ready-to-exploit and bug-free, i.e. the time associated with the development of the numerical code and bug fixing are not included. Also, the time expend for re-running of simulations is also not included. Finally, the total simulation time has to be put in perspective of the CPU specifications used for each code. It represents the parallelisation capacity applied on the calculation process to reduce its computation time. As such, even if BEMT-CFD and Blade-Resolved CFD have similar total simulation time, Blade-Resolved CFD numerical model has a significantly higher cost.

Table 11: Comparison of computation time for different models (Edinburgh generic turbine at TSR = 7 - Flow only case)

Event		BEMT	BEMT-CFD	Blade-Resolved CFD
Simulation Time	Pre-processing	20 mins	9 hours	24 hours
	Computation	5 secs	2 days for 12 s	3 days
	Post-processing	5 mins	2 hours	2 hours
	Total Time	**25 mins**	**2.5 days**	**4 days**
CPU Specifications	Processor	Intel i7	Linux Cluster	Linux Cluster
	Number of cores	**6-cores**	**36-cores**	**224-cores**
	RAM	16GB	4GB per core	60GB per node
Simulation Specification	Spin-up Duration	-	14 s (Convection of the wake along the domain)	30 s
	Time step value	Steady	0.002 s	0.004 s (2° rotation per time step)

Table 12: Comparison of computation time for different models (Edinburgh generic turbine at TSR = 7 - Flow + Wave case for an output of 30 seconds)

Event		BEMT	BEMT-CFD	Blade-Resolved CFD
Simulation Time	Pre-processing	30 mins	9 hours	24 hours
	Computation	50 mins	5.5 days	6 days
	Post-processing	5 mins	3 hours	3 hours
	Total Time	**1.5 hours**	**6 days**	**7 days**
CPU Specifications	Processor	Intel i7	Linux Cluster	Linux Cluster
	Number of cores	**6-cores**	**36-cores**	**224-cores**
	RAM	16GB	4GB per core	60GB per node
Simulation Specification	Spin-up Duration	-	Start from previous converged solution	
	Time step value	0.01 s	0.002 s	0.004 s (2° rotation per time step)

The pre-processing time refers to the activities performed by the modeller prior to the commencement of the simulations. This means the time dedicated to the discretization of the blade geometry and calculation of geometrical parameters, according to the approach. Also, setting up the domain and boundary conditions.

Computation time refers to the time taken by the simulation technique to make the calculations. This is associated with the time taken by the solver to reach a converged solution.

Post-processing time is the time elapsed between the end of the simulations until the data is ready for comparison. Typically, this would include the extraction of the data from the source files, visualisation of the output plots and processing of the time-series data to obtain additional parameters and the average results.

In addition to this comparison of time cost, a discussion on the advantages and disadvantages of each model is provided later on. When considering a specific task, comparing the capabilities of each approach with regard to their cost may provide useful insights to select the best suited one.

7 Discussion and conclusions

Within the purview of this work, an attempt has been made to characterize and simulate the complex flow environment that tidal turbines are subjected to. Such an implementation has been performed for 3 different numerical model constructs of varying complexity. A cross-comparison of the performance of these models for same loading cases have been considered, and it has also been compared along with experimental tank test results. The outcome, limitations and conclusions from this work are summarized hereafter.

7.1 Critical assessment of the numerical models

The Blade-Resolved CFD model provides a comprehensive representation of a turbine rotor, allowing detailed estimates of pressure loads on the blades and wake development behind the turbine. However, due to the complexity of the model and the small time step required to run it, it becomes a very costly tool. Indeed, the wake directly influences the loads applied on the turbine and one has to wait until it is fully developed to get trustworthy results. Its use has to be put in perspective with the objectives of the study before selecting this approach. Moreover, it has been identified that Blade-Resolved CFD model is facing difficulties with the model scale of the turbines due to the transition between laminar and turbulent flow. The Reynolds number, representative of the flow state, is lowered compared to full scale leading to different viscous behaviour. It is a commonly known issue when studying propellers as well. As such, it would be interesting to consider full scale CFD calculations for a comparison to scaled results of tank tests using ITTC 78 [46] or any other relevant extrapolation method. Full scale experimental data would enable to go even further in the calibration of the numerical model. In the context of RealTide, the data monitoring planned on D12 turbine in operation will provide valuable inputs to do so. Flow measurements in parallel with blades loads and performance monitoring will be used to enhance the reliability of Blade-Resolved CFD model.

BEMT is a simplified numerical model, and hence the level of detail available in the model is the least among all the models used. This also results in much lower computational time, wherein the computational effort required is measured in the order of minutes, instead of days. The BEMT model used here is a modified one, taking into account part of the realistic behaviour of the inflow - the spatial variation and the unsteady nature of the inflow. However, the model is still quasi-static and sensitive to the turbulent fluctuations of the inflow velocity field. Therefore, the energy within the turbulent structures is not completely captured by the BEMT model. Consequently, the associated contributions to the blade forces are affected and the BEMT will not be able to compute the wake field of the flow. The effect is more pronounced for very low TSRs and very high TSRs. These limitations of the model must be accounted for when choosing such a model for gain in computational time and effort.

The BEMT-CFD model can be considered a hybrid model which involves CFD and ALM, which in turn involves BEMT and the model which represents the interaction between the rotor and the surrounding flow (body forces). Acceptable accuracy is computed for variables like torque, however, for the case of the thrust, the error increases for turbines with largest hub radius like in the case of the IFREMER Sabella D12 turbine. Thus, improvement of the rotor-surrounding flow interaction model, which modifies the local velocity field, or modelling the rotor hub are expected to be used. Concentrated load distribution along the blades can also be estimated, but it is restricted to the number of blades elements used. By using the LES turbulence model, the BEMT-CFD model can represent the wake development and the flow interaction between diverse turbines, for the cases of tidal farms, however, the computational time consumption is mostly due to the use of the LES turbulence model.

7.2 Main outcomes

The work presented in this paper is intended to provide a benchmark database for computation and design of tidal turbines. It could be used as a reference for validating new numerical approaches, as well as a guideline for tidal turbine designers. The results have been presented for a generic turbine as well as for a commercial turbine.

The numerical predictions for models of increasing complexity have been inter-compared by modelling the same test cases, and validating the results against the measured response of scale model turbines run under the

same test conditions. This set of results will help users identify which numerical simulation tool is optimal for a given task, with in the constraints of complexity and cost.

The numerical tools and techniques developed as part of the RealTide project have been tuned to adapt to the flow environment surrounding a tidal turbine. These are expected to be used for further comparative studies of turbine performance, and eventually in the design of commercial turbine blades. The comparison study presented within this work also provides a better understanding about how the 'predictions' from the numerical models match up against the 'observations' from the experimental models. Subsequent work in the RealTide project is focused on how these predictions and observations contrast against the true behaviour of the turbine in real sea conditions.

7.3 Limitations

The simulation results from all the models are presented for 3 cases with current only and for 1 case with current and waves. While this gives a good framework for comparison, more cases could be compared to obtain a more holistic overview of the results. The cases with very low TSRs and very high TSRs are those where a simplistic model like BEMT can provide large discrepancies. It could be interesting to compare the results for such rotational speeds.

The main limitation of the BEMT-CFD model is that its ALM was unable to capture realistic values of thrust for the Sabella D12 turbine. This type of tidal turbine has a particular geometrical characteristic for which the blades and hub do not resemble those of a wind turbine. The rotor model originally implemented in the open-source program SOWFA was oriented for wind turbine applications.

None of the numerical models considered have implemented a free-surface, so waves cannot be correctly implemented. To represent wave forcing, the horizontal component of the wave orbital velocity, based on linear wave theory, has been imposed as a boundary condition. This is adequate for the BEMT model, but is unrealistic for the BEMT-CFD and Blade-Resolved CFD models, as it artificially moves the entire fluid domain at the wave frequency. This approach can only be used for simple plane harmonic waves following the flow. To correctly implement waves the models require a free-surface and means of driving waves through the domain.

The spectral analysis showed that the presence of a support pillar has a significant impact on the turbine response. This has been identified as a limitation in the numerical simulations analysed. The BEMT-CFD and Blade-Resolved CFD models are able to represent the support structures within in the model domain. This level of complexity was outside the scope of the remit for the RealTide project, but needs to be considered for future development.

Finally, in the Blade-Resolved CFD, due to the use of RANSE method in the calculations, the turbulence initiated at the inflow boundary is modelled as being latent. The absence of friction or generator at the inlet lead to a flow without the large scales turbulent structures being generated upstream. This numerical phenomenon tends to remove the turbulence effect on the turbine loads. Therefore the turbulence method of computation may be improved to tackle this point.

7.4 Future improvements

Detailed modelling of Blade-Resolved CFD model enabled to quantify the influence of the hub effect on the turbine performance, especially for D12 turbine. It highlighted the importance of taking it into account, in particular when considering thrust. As such, possible improvements of BEMT and BEMT-CFD could be the development of modules enabling the consideration of the turbine structure (nacelle and support) in addition to the blades. In parallel, an improved model for body forces distribution of the ALM in the BEMT-CFD is expected to be used in order to capture more realistic flow behaviour around the blades. Also, the consideration of a free surface is expected to be presented in the CFD models.

In terms of turbulence, the use of Detached Eddy Simulation (DES) instead of RANSE method could dramatically improve the turbulence resolution in the flow for Blade-Resolved CFD model. It will be investigated later on in the context of RealTide project. However, one has to keep in mind that it goes with an important numerical cost increase. Therefore, depending on the required outputs, it may not be relevant for all applications.

Finally, the inflow representation in the BEMT model could be further enhanced to include semi-empirical models that account for dynamic stall effects. Such models work based on experimentally or numerically determined constants which are unique to the blade geometry. A further improvement to the BEMT model would be accounting for the impact of such dynamic stall events.

7.5 Recommendations: design applications of numerical codes

The comparison work presented in this paper has identified some of the key strengths and drawbacks of the studied numerical simulation approaches. The following is a summary of these findings, that we hope will help the reader identify the numerical tool most suited for a given task.

The very low numerical cost of the BEMT method makes it the optimal choice for early design stage or design optimization tools. It enables to obtain a first guess of the optimal TSR value and associated performance. In the detailed design phase, the Blade-Resolved CFD provides critical inputs for the structural analysis. It enables to obtain the pressure field and mean forces on the blade surfaces as well as fatigue loads. BEMT based line actuator models do not give an accurate representation of the blade forces over the entire blade surface area. Moreover, the flow and wake are also fully modelled in CFD and can be very helpful to verify the relevance of the blade shape with regard to its interaction with the flow. However, this approach goes along with a very important computational cost. Therefore, it should be selected only when detailed information are needed or for design validation.

BEMT-CFD coupled system comes in-between the two previous methods. It gives a good representation of the wake field for a reasonable cost as it uses BEMT to simulate the turbine presence. It is well adapted to study the flow interactions between diverse turbines in tidal turbine farms. The use of Blade-Resolved CFD models for tidal farms would mean an impracticable use due to the high computational cost demand. Since the turbine in the BEMT-CFD model is represented as a line actuator, this model can also provide line pressure distributions over the blade.

These recommendations highlight the wide range of applications for numerical models in the design of tidal turbine blades. Moreover, it also confirms the need for the user to define clearly the objectives of the study to select the most adapted tool. A thorough assessment of the work previous to any calculations will enable to get the best of the numerical tools.

References

[1] Ocean Energy Forum (2016). *Ocean Energy Strategic Roadmap: Building Ocean Energy for Europe*, `https://webgate.ec.europa.eu/maritimeforum/en/frontpage/1036`.

[2] S. Draycott, G. Payne, J. Steynor, A. Nambiar, B. Sellar, V. Venugopal (2019). *An experimental investigation into non-linear wave loading on horizontal axis tidal turbines*, Journal of Fluids and Structures, 84, 199-217.

[3] D. Ingram (2011), *Protocols for the Equitable Assessment of Marine Energy Converters*, Edinburgh, UK, The University of Edinburgh.

[4] RealTide Project (2018). *Deliverable D1.1 Increased Reliability of Tidal Rotors: Failure Mode and Effects Analysis (FMEA)* [Online] Available at: `https://www.realtide.eng.ed.ac.uk/`.

[5] I.G. Bryden, S.J. Couch, A. Owen, G. Melville (2007). *Tidal current resource assessment*, Proceedings of the Institute of Mechanical Engineers, Part A: Journal of Power and Energy, 2, 125-154.

[6] M. Rahimian, J. Walker, I. Penesis (2017). *Numerical assessment of a horizontal axis marine current turbine performance*, International Journal of Marine Energy, 20, 151-164.

[7] T.M. Nevelainen, C.M. Johnstone, A.D. Grant (2016). *A sensitivity analysis on tidal stream turbine loads caused by operational, geometric design and inflow parameters*, International Journal of Marine Energy, 16, 51-64.

[8] A. Creech, W. Fruh, A.E. Maguire (2015). *Simulations of an Offshore Wind Farm Using Large-Eddy Simulation and a Torque-Controlled Actuator Disc Model*, Surveys in geophysics.

[9] I. Masters, A. Williams, T.N. Croft, M. Togneri, M. Edmunds (2015). *A Comparison of Numerical Modelling Techniques for Tidal Stream Turbine Analysis*, Energies, 8, 7833-7853.

[10] U. Ahmed, D.D. Apsley, I. Afgan, T. Stallard, P.K. Stansby, *Fluctuating loads on a tidal turbine due to velocity shear and turbulence: Comparison of CFD with field data*, Renewable Energy, Volume 112, 2017, Pages 235-246, ISSN 0960-1481, https://doi.org/10.1016/j.renene.2017.05.048.

[11] C.R. Vogel, R.H.J. Willden, G.T. Houlsby (2018). *Blade element momentum theory for a tidal turbine*, Ocean Engineering, 169,215-226.

[12] M. Sousounis, J.P. Tomy, S. Paboeuf, J.K.H. Shek (2019). *Tide-to-wire model development for realistic tide environments*, Proceedings of the 13th European Wave and Tidal Energy Conference, Naples, Italy.

[13] G.T. Scarlett, I.M. Viola (2020). *Unsteady hydrodynamics of tidal turbine blades*, Renewable Energy, 146, 843-855.

[14] RealTide Project (2019). *Deliverable D3.1 Generalised tide-to-wire model.* [Online] Available at: `https://www.realtide.eng.ed.ac.uk/`.

[15] M. Churchfield, S. Lee (2012). *Simulator for Wind Farm Applications - SOWFA*, National Renewable Energy Laboratory, NREL (USA).

[16] J. Sorensen, W. Shen (2002). *Numerical Modeling of Wind Turbine Wakes*, J. Fluids Eng, 124, 393-399.

[17] OpenFOAM (2015). *User Guide, Version 2.4.0*, OpenFOAM Foundation Ltd.

[18] L. Martinez, S. Leonardi (2012). *Wind Turbine Modeling for Computational Fluid Dynamics*, National Renewable Energy Laboratory, NREL (USA).

[19] D. Sale, A. Aliseda (2016). *The flow field of a two-blades horizontal axis turbine via comparison of RANS and LES simulations against experimental PIV flume measurements*, In: Proceedings of the 4th Marine Energy Technology, Washington DC (USA).

[20] P. Fleming, S. Lee, M. Churchfield, A. Scholbrock, J. Michalakes, K. Jonhson, P. Mariarty (2013). *The SOWFA Super-Controller: A High-Fidelity Tool for Evaluating Wind Plant Control Approaches*, National Renewable Energy Laboratory, NREL (USA).

[21] RealTide Project (2019). *Deliverable D3.2 Blade resolved CFD modelling of tidal turbines.* [Online] Available at: `https://www.realtide.eng.ed.ac.uk/`.

[22] I.A. Milne, A.H. Day, R.N. Sharma, R.G.J. Flay (2016). *The characterisation of the hydrodynamic loads on tidal turbines due to turbulence*, Renewable and Sustainable Energy Reviews, 56, 851-864.

[23] L.E. Myers, A.S. Bahaj (2012). *An experimental investigation simulating flow effects in first generation marine tidal current energy converter arrays*, Renewwable Energy, 37, 28-36.

[24] N.-S. Cheng (2007). *Power-law index for velocity profiles in open channel flows*, Advances in Water Resources, 30, 1775-1784.

[25] D.R. Noble, T. Davey, H.C.M. Smith, P. Kaklis, A. Robinson, T. Bruce (2015). *Characterisation of spatial variation in currents generated in the FloWave Ocean Energy Research Facility*, Proceedings of the 11th European Wave and Tidal Energy Conference, Nantes, France, pp. 1-8.

[26] R.E. Baddour, S. Song (1990). *On the interaction between waves and currents*, Ocean Engineering, 17, 1-21.

[27] A. Vallgren, E. Lindborg (2011). *The enstrophy cascade in forced two-dimensional turbulence*, Journal of Fluid Mechanics, 671, 168-183.

[28] B.G. Sellar, G. Wakelam, D.R. Sutherland, D.M. Ingram, V. Venugopal (2018). *Characterisation of tidal flows at the European Marine Energy Centre in the absence of ocean waves*, Energies, 11, 176; doi:10.3390/en11010176.

[29] D. Ingram, R. Wallace, A. Robinson, I. Bryden (2014). *The design and commissioning of the first , circular, combined current and wave test basin*, In OCEANS 2014, pages 1-7, New York, 2014. IEEE.

[30] G.S. Payne, T. Stallard, R. Martinez (2017). *Design and manufacture of a bed supported tidal turbine model for blade and shaft load measurement in turbulent flow and waves*, Renewable Energy, 107, 312-326.

[31] B. Gaurier, G. Germain, J.-V. Facq, T. Bacchetti (2018). *Wave and current flume tank of IFREMER at Boulogne-sur-mer. Description of the facility and its equipment.* [Online] Available at: `https://archimer.ifremer.fr/doc/00470/58163/`.

[32] M. Churchfield, Y. Li, P. Moriarty (2013). *A large eddy simulation study of wake propagation and power production in an array of tidal-current turbines*, Philosophical Transactions of the Royal Society A, 371, 1-15.

[33] `https://epsrc.ukri.org/research/ourportfolio/themes/energy/programme/what-the-energy-programme-funds/supergen-programme/`.

[34] S.G. Parkinson, W.J. Collier (2016). *Model validation of hydrodynamic loads and performance of a full-scale tidal turbine using Tidal Blade*, International Journal of Marine Energy, 16, 279-297.

[35] B. Gaurier, G. Germain, G. Pinon (2018). *How to correctly measure turbulent upstream flow for marine current turbine performance evaluation?* In: Proceedings of the 3rd International Conference on Renewable Energies Offshore. Lisbon, Portugal, 2018.

[36] I. Abbot, A. von Doenhoff, *Theory of wing sections: including a summary of airfoil data*, Dover Publications Inc., New York, 1959.

[37] P. Jha (2015). *Characterization of Wake Turbulence in a Wind Turbine Array Submerged in Atmospheric Boundary Layer Flow*, PhD thesis, The Pennsylvania State University (USA).

[38] I.A. Milne, R.N. Sharma, R.G.J. Flay, S. Bickerton (2010). *The role of waves on tidal turbine unsteady blade loading*, 3rd International Conference on Ocean Energy, 6 October, Bilbao.

[39] S. Draycott, D. Noble, T. Davey, J. Steynor, D.M. Ingram (2017). *Application of complex wave and current conditions in a laboratory environment*, In A. Lewis, editor, Proceedings of the 12th European Wave and Tidal Energy Conference, pages 890/1–890/8, University College Cork, Ireland, 2017.

[40] S. Draycott, A. Nambiar, B. Sellar, T. Davey, V. Venugopal (2019). *Assessing extreme loads on a tidal turbine using focused wave groups*, Renewable Energy, 135, 1013-1024.

[41] S. Draycott, J. Steynor, A. Nambiar, B. Sellar, V. Venugopal (2019). *Experimental assessment of tidal turbine loading from irregular waves over a tidal cycle*, Journal of Ocean Engineering and Marine Energy, 5, 173-187.

[42] P. D. Welch (1967). *The use of fast Fourier transforms for the estimation of power spectra: A method based on time averaging over short modified periodograms*, IEEE Transactions on Audio and Electroacoustics, 15, 70-73.

[43] G.S. Payne, T. Stalllard, R. Martinez, T. Bruce (2018). *Variation of loads on a three-bladed horizontal axis tidal turbine with frequency and blade position*, Journal of Fluids and Structures, 83, 156-170.

[44] D.R. Noble, S. Draycott, A. Nambiar, B.G. Sellar, J. Steynor, A. Kiprakis (2020). *Experimental assessment of flow, performance, and loads for tidal turbines in a closely-spaced array*, Energies, 13, 1977; doi:10.3390/en13081977.

[45] M. Churchfield, S. Schreck, L.A. Martinez-Tossas, C. Meneveau, P.R. Spalart (2017). *An Advanced Actuator Line Method for Wind Energy Applications and Beyond*, National Renewable Energy Laboratory, NREL (USA).

[46] International Towing Tank Conference (2008). *Performance, Propulsion - 1978 ITTC Performance Prediction Method*, ITTC - Recommended Procedures and Guidelines (Rev01 - 2008). Available at : `https://ittc.info/media/1593/75-02-03-014.pdf`.